First Wall and Cavity Design Studies for a Light Ion Beam Driven Fusion Reactor

G.A. Moses, S.I. Abdel-Khalik, D. Drake, R. Engelstad, G.L. Kulcinski, R. Lewis, E. Lovell, T. McCarville, L. Peranich, R.R. Peterson, M. Ragheb, R. Spencer

October 1979

UWFDM-320

FUSION TECHNOLOGY INSTITUTE

UNIVERSITY OF WISCONSIN

MADISON WISCONSIN

First Wall and Cavity Design Studies for a Light Ion Beam Driven Fusion Reactor

G.A. Moses, S.I. Abdel-Khalik, D. Drake, R. Engelstad, G.L. Kulcinski, R. Lewis, E. Lovell, T. McCarville, L. Peranich, R.R. Peterson, M. Ragheb, R. Spencer

Fusion Technology Institute
University of Wisconsin
1500 Engineering Drive
Madison, WI 53706

http://fti.neep.wisc.edu

October 1979

UWFDM-320

Issued by Sandia Laboratories, operated for the United States Department of Energy by Sandia Corporation.

SF 1004-DF(11-77)

FIRST WALL AND CAVITY DESIGN STUDIES

FOR A LIGHT ION BEAM DRIVEN FUSION REACTOR

by

G. A. Moses, S. I. Abdel-Khalik, D. Drake,
R. L. Engelstad, G. L. Kulcinski, R. Lewis,
E. Lovell, T. McCarville, L. Peranich,
R. R. Peterson, M. M. Ragheb, R. Spencer

September 1979

UWFDM-320

Fusion Engineering Program
Nuclear Engineering Department
University of Wisconsin

This work was supported by Sandia Laboratories under contract DSG/06-9329.

Abstract

Cavity and first wall designs for light ion beam fusion reactors are reported. This effort includes parametric analysis of the cavity gas response as a function of the gas temperature and gas type, the first wall mechanical response as a function of the wall material and structural design, the first wall thermal response as a function of cavity gas type and wall thickness. Also included are neutronics and time dependent radiation damage studies of the first wall, taking account of neutron interactions in the pellet. There is an assessment of the cavity gas recirculation system with possible design alternatives. A novel cavity design that utilizes the effect of blast waves in a gas with a strong density gradient is introduced. Basic conclusions regarding the viability of conservative cavity design options are listed.

I. Introduction and Overview

A new approach to inertial confinement fusion (ICF) that is drawing increasing attention is the use of intense beams of light ions, such as 5-10 MeV protons, focussed onto a fusion target. Light ions generate no energetic electrons or hard X-rays upon interacting with the target and presumably deposit their energy according to the classical ion range-energy theories. This is a significant advantage over lasers and relativistic electron beams that depend upon so-called anomalous absorption or enhanced absorption to couple effectively to the target.

Significant advances have recently been made in the study of light ions for fusion applications. It has been demonstrated that light ion beams can be generated using the "pulsed power/diode" technology that has been under investigation at Sandia Laboratory, Albuquerque, and at other laboratories for several years.[1] It has also been demonstrated that these light ion beams can be propagated in ionized channels at significant power densities.[2] For fusion experiments it is proposed that the target be placed at a common intersection of many such ionized channels, each of which leads back to an individual diode. These notions will be tested experimentally on the PBFA-I facility at Sandia, Fig. I-1.

With these advances in light ion beam technology and the construction of a large light ion beam fusion experiment currently in progress, it is appropriate to begin exploring the technical problems associated with development of a light ion beam fusion reactor. The results of such fusion

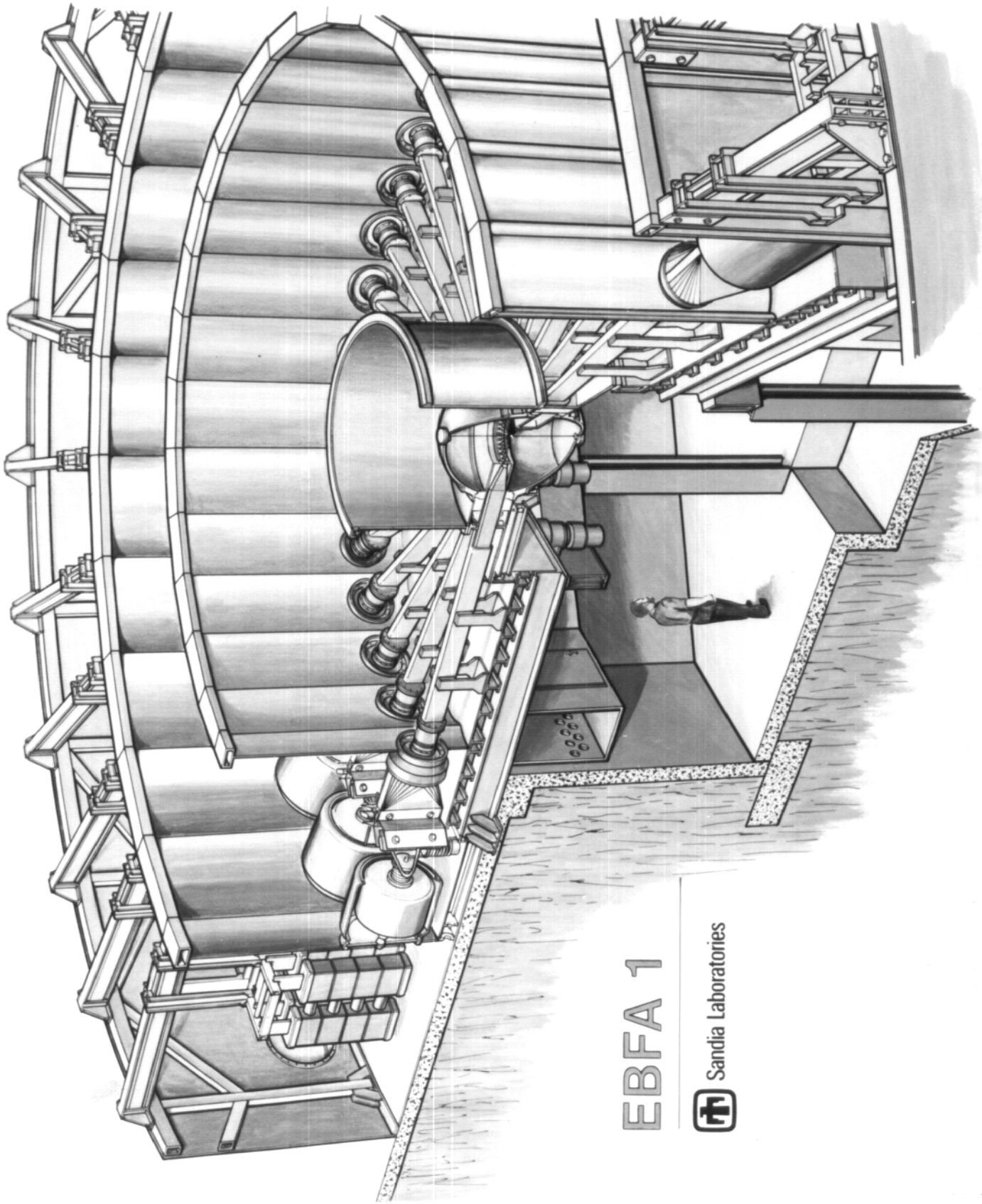

Fig. I-1

technology studies along with the physics experiments to be completed in the next 5-6 years form a basis from which future decisions can be made regarding the attractiveness of this particular fusion concept for reactor applications.

The light ion beam (LIB) reactor study reported here represents an initial step in the building of this technical base from which the potential of LIB fusion as a reactor can be assessed. The emphasis of this study is on the design of the reactor cavity and first wall. Although ultimate conclusions must await more investigation and analysis of the entire reactor system, this study has begun to uncover many attractive features and potential problems related to LIB reactor development. The theme of this work is two-fold. First, a reactor cavity and first wall that is conservative in concept is designed. This design uses conventional materials and standard engineering design features. Second, innovative designs that take advantage of the unique features of LIB fusion but are more speculative in nature are investigated.

Conservative Approach

A major feature of the LIB fusion approach under investigation in this study is the presence of a gas in the reactor cavity to provide the medium for ionized channel formation. These ionized channels serve to transport the ion beams from the diodes to the fusion target. The formation of these channels might be by laser ionization followed by a capacitor discharge along the channel.[3] However the emphasis in this study is on the overall behavior of this gas in the cavity and not on the details of channel formation. Questions that are addressed include:

(1) What type of gas is best suited for this purpose?

(2) What is the response of this gas to the pellet explosion?

(3) What heat flux and overpressure does this gas transmit to the first wall following the pellet explosion?

(4) At what temperature should this gas be operated?

(5) At what rate must the gas be pumped from the cavity?

(6) What does the gas recirculation system look like?

For the purposes of ionized channel formation and beam transport it is anticipated that the gas pressure will be 10-100 torr, or more appropriately, a number of density of 3.5×10^{17} - 3.5×10^{18} cm^{-3}. At this density, most gases heavier than He will very effectively shield the first wall from the fusion target debris and X-rays. However, the rapid deposition of these debris and X-rays into the gas will create a fireball and resultant blast wave and these will propagate to the first wall. The major issues concerning the first wall are the following:

(1) What is the overpressure and heat flux incident on the first wall?

(2) Under what circumstances can the first wall be designed to accept this overpressure and heat flux using conventional materials and engineering design techniques?

Another problem that is common to all DT fusion reactors is neutron radiation damage to the first wall and blanket. Hence other questions of importance are:

(3) Can a first wall be designed that meets the requirements of thermal response, mechanical response and radiation damage response at an acceptable cavity radius?

(4) Does the pulsed nature of the radiation affect the response of the wall?

Each of these questions has been studied parametrically. However, to avoid scores of unrelated calculations a basic reactor cavity and first wall configuration is chosen to serve as the focal point for calculations. This is shown in Fig. I-2 and Fig. I-3. The reactor cavity bears a striking resemblance to the PBFA facility shown in Fig. I-1. This is consistent with a conservative design approach.

Depending on the cavity gas type the first wall must withstand a significant overpressure, on the order of several atmospheres, along with (or without) a substantial heat flux. For the first wall design in this study it is best to minimize the thermal loading because then the wall may be actively cooled to low temperature without a great loss in the thermal efficiency of the entire system. This low temperature operation can lead to reduced swelling due to radiation damage and hence to a longer wall lifetime. The cellular wall construction is shown in the insert on Fig. I-3 to be panels of two plates with stiffening supports in between them. These supports form channels that coolant may be pumped through to actively cool the wall. The panels are supported from behind by a rigid structure frame. This design concept allows the first wall structural analysis to be simplified to a study of the response of a single panel to blast overpressure. Stainless steel has been chosen as the structural material because there is a great amount of information and technology development associated with its production and fabrication. The poor thermal properties of stainless steel will not be important in this design, so long as the heat flux from the cavity gas to the

LIGHT ION BEAM REACTOR CAVITY AND FIRST WALL

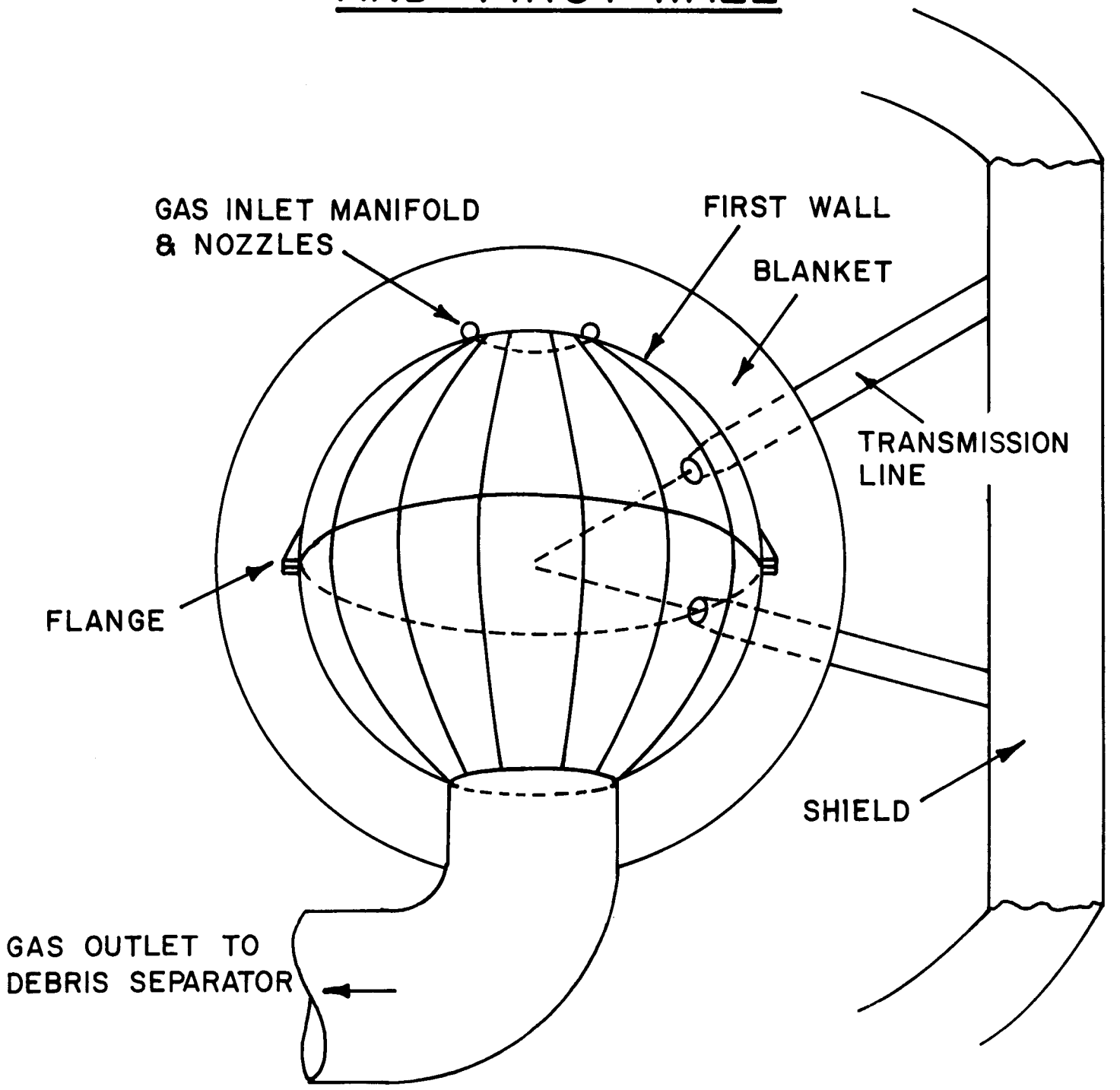

Fig. I-2

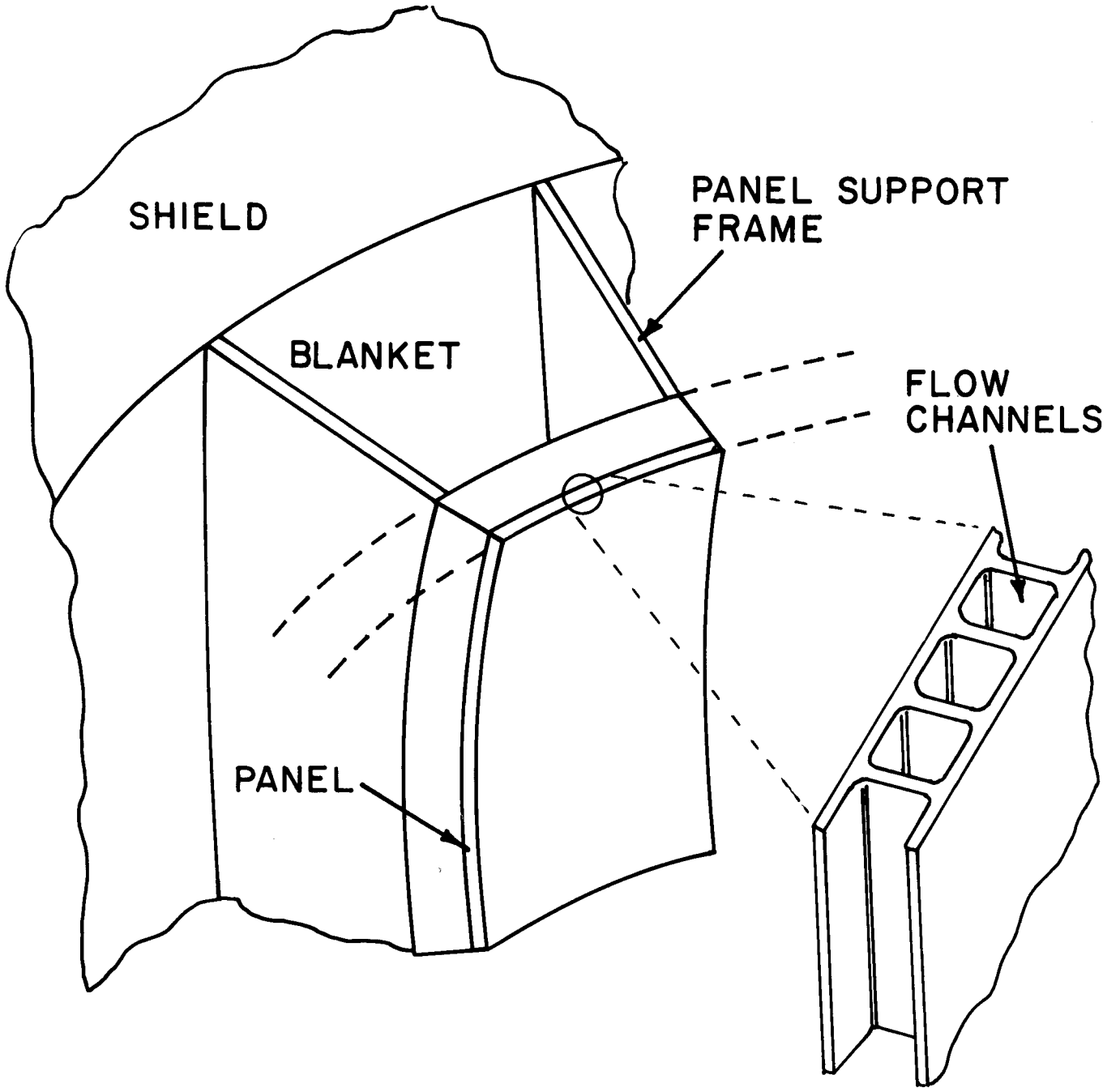

FIRST WALL PANEL

Fig. I-3

first wall is minimized. Table I-1 lists some typical parameters for the first wall assuming that the maximum overpressure is 4 atmospheres. Two different stress limits of 20 ksi and 10 ksi are used to demonstrate that the mechanical overpressure on the first wall can be accommodated using conventional materials and design techniques. This is a very important result.

The cavity gas response to the microexplosion is sensitively dependent on the type of gas in the cavity and the ambient temperature of this gas. Monatomic gases such as argon are highly transparent to radiation at frequencies lower than the transparency temperature, which is high (1.5 eV) for noble gases. As the fireball created by the microexplosion expands outward it cools down until it reaches its transparency temperature. It then turns from a surface to a volume radiator and "leaks" the fireball energy through the shock front to the first wall, Fig. I-4. This reduces the overpressure experienced at the first wall when the shock arrives but it significantly increases the thermal loading on the wall. Diatomic gases such as nitrogen do not exhibit such a high transparency and they retain the explosion energy in the fireball behind the shock front. Hence the overpressure at the first wall is greater but the heat flux is substantially reduced. Table I-2 gives the results of two fireball calculations using 50 torr of argon and 50 torr of a "diatomic argon" gas.* The substantial differences in these two results points out the importance of the cavity gas type to the wall response and hence the wall design. For the diatomic gas the heat flux at the wall is very small hence the thermal response of the

---

*The "diatomic argon" was modelled using the argon data generated by the MFP code but with the restriction that the radiation mean free path not go above 50 cm even when the gas cools below the transparency temperature.

Table I-1

First Wall Mechanical Design Parameters

Cavity Radius = 400 cm

Gas Duct Radius = 170 cm

Plate Height = 420 cm

Maximum P_w = 58.8 psi

# of Panels/ Hemisphere	Front Plate Thickness (cm)	Total Plate Thickness (cm)	
		20 ksi	10 ksi
32	0.5	5.61	11.86
32	0.75	3.74	7.91
32	1.0	2.80	5.93

$T > T_{transparent}$

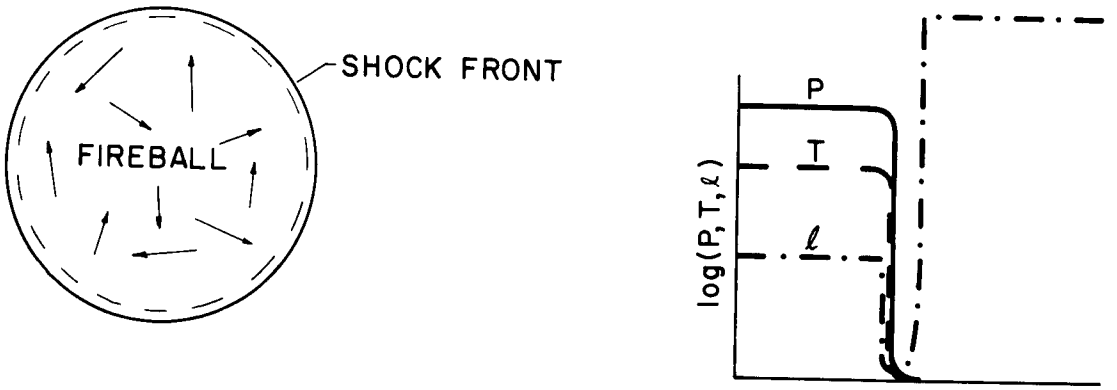

$T < T_{transparent}$

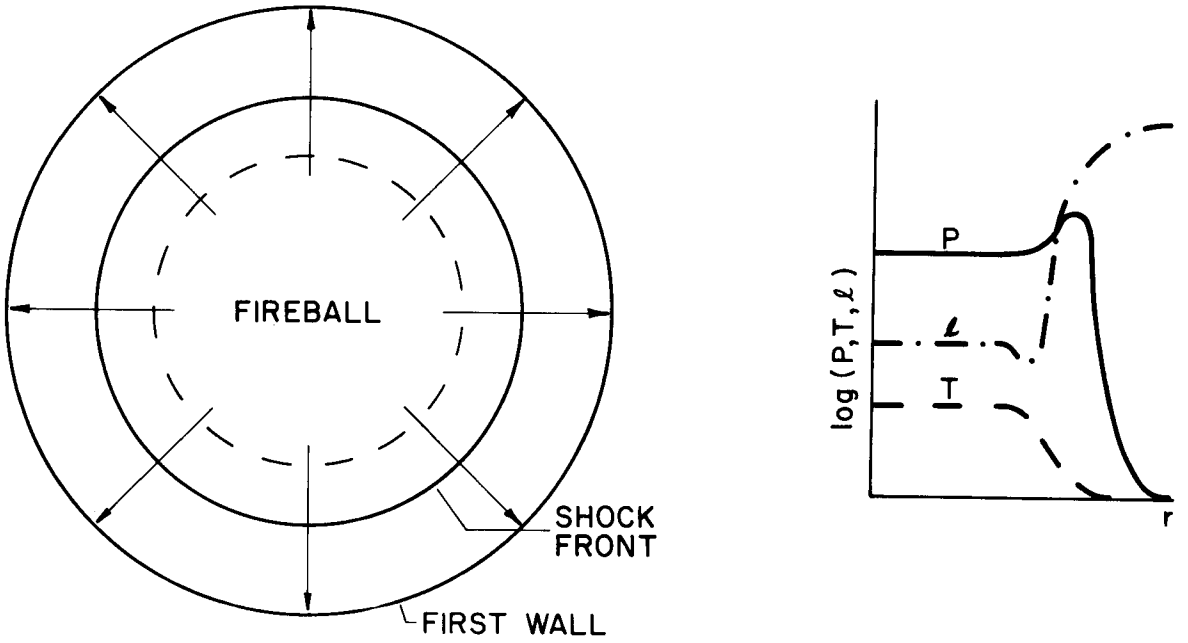

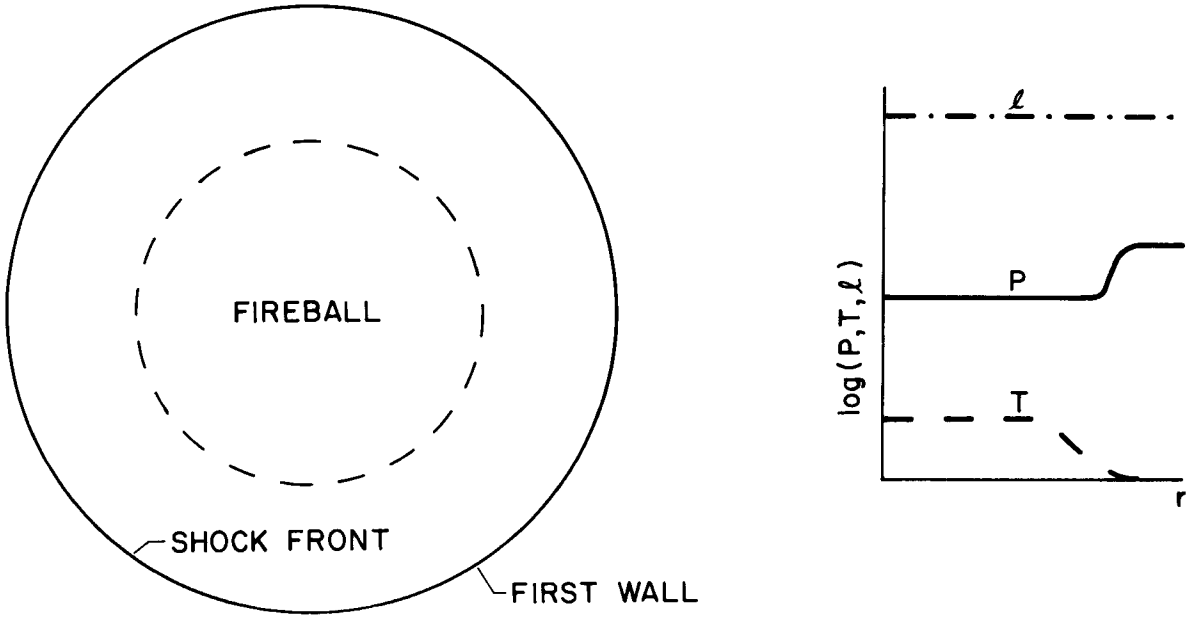

Fig. I-4

Table I-2

Fireball Calculations for Argon and

"Diatomic Argon" Cavity Gases

	Argon	"Diatomic Argon"
Gas Pressure (@ 0°C)	50 torr	50 torr
Energy Deposited into Gas	30 MJ	30 MJ
Initial Gas Temperature	1160°K	1160°K
Wall Radius	4m	4m
Maximum Overpressure	1.5 Atm	2.75 Atm
Maximum Heat Flux	18 kW/cm^2	0.13 kW/cm^2
Energy Radiated to Wall in 5 ms	7.5 MJ	0.15 MJ
First Wall Surface Temperature Rise @ 10 Hz	317°C	2.7°C

wall is benign. This is a very positive result since it allows the use of stainless steel as a structural material even though it has a poor figure of merit with regard to transient thermal stresses.

Since there is little energy transferred to the first wall, the heat must be removed by pumping the gas from the cavity. The gas flows through the inlet and outlet ducts shown at the top and bottom of the cavity in Fig. I-2. From the outlet duct it must flow through a debris separator before going to the heat exchanger. Before entering the cavity the gas flows through a suppression chamber that damps the shock wave that would otherwise propagate back up the duct following the microexplosion. Depending on the mass flow rate through the cavity, this gas exits at a very high temperature in relation to state-of-the-art gas heat exchangers. Typical exit temperatures are from 1000°K-8000°K. Table I-3 shows some typical parameters. Current heat transfer equipment operates at <1000°K. To establish this low effective exit temperature in the cavity gas requires prohibitively large mass flow rates and pumping power. Hence, this gas must be mixed with a lower temperature, higher pressure, gas stream before entering the heat exchanger. This is shown in Fig. I-5. A detailed design of this system was not done in this study. With this mixing included the remainder of the gas recirculation cycle can be quite similar to that of an HTGR, and the technological extrapolations can be isolated to a small fraction of the total system.

Neutronics calculations that include interactions in the fusion pellet indicate that the time averaged values of dpa and gas production in the stainless steel first wall are not reduced by more than about 20% when compared

Table I-3

Cavity Gas Flow Parameters*

Inlet Temp. (°K)	Outlet Temp. (°K)	Ave. Cavity Temp. (°K)	Power Radiated[1] to First Wall (MW)	Mass Flow Rate (g/sec)	Velocity[2] (cm/sec)
573	587	580	66	2.7×10^7	1.1×10^5
573	1747	1160	75	3.3×10^5	1.4×10^3
573	11031	5802	147	2.5×10^4	1.0×10^2
573	15673	8123	203	4.5×10^3	19.

*30 MJ/shot deposited into 50 torr of argon at the rate of 10 Hz.

(1) Computed using the FIRE + MFP fireball simulation code.

(2) At the midplane of a 4m cavity.

CAVITY GAS RECIRCULATION SYSTEM

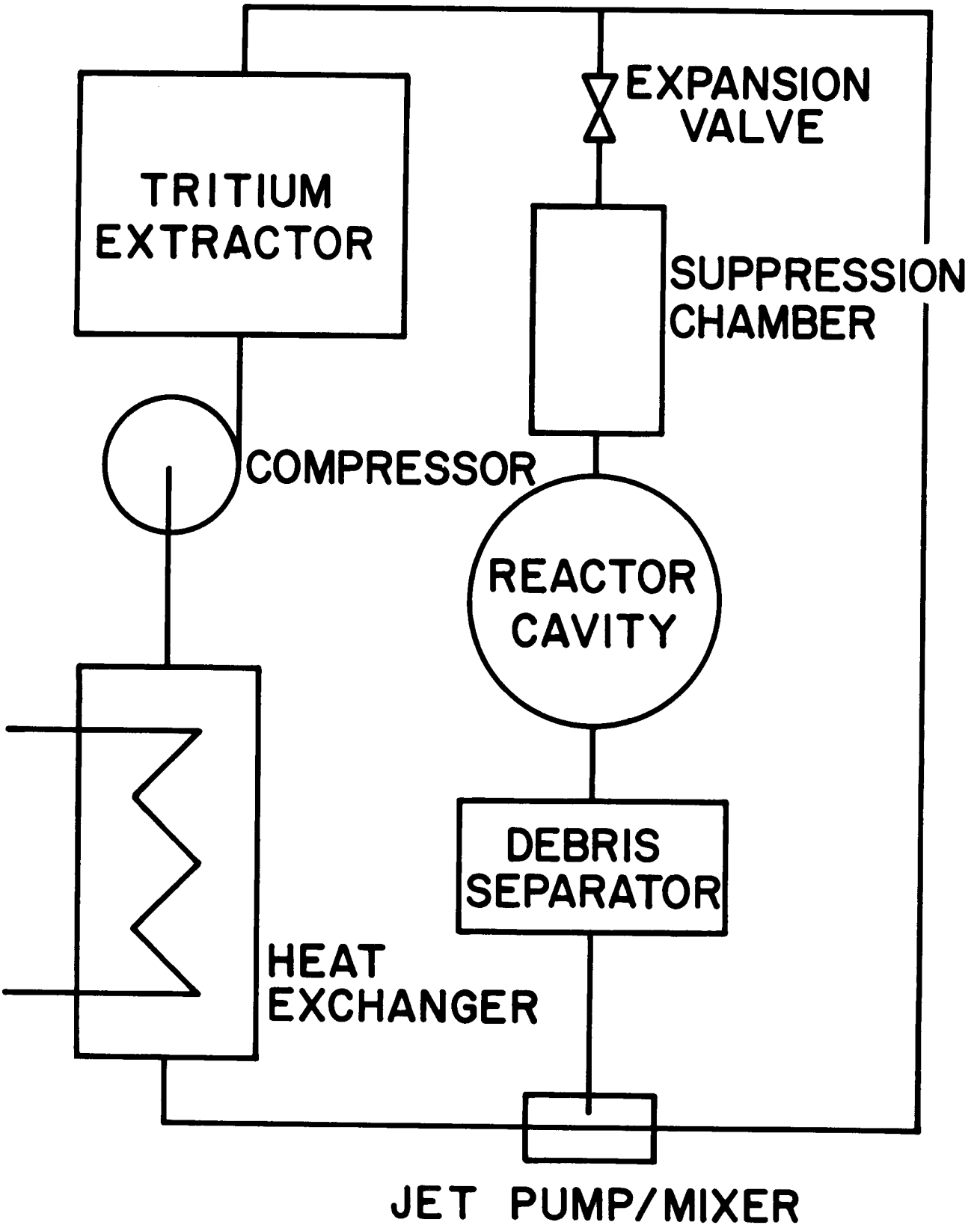

Fig. I-5

to a "pure" 14.1 MeV neutron source. Futhermore, the tritium breeding function in the blanket is affected very little by neutron downscattering in the pellet. However time dependent analyses show that the radiation damage done in the first wall and throughout the blanket is done at a high damage rate. Hence rate dependent effects are not substantially mitigated by the presence of the pellet and this leaves open the questions regarding first wall lifetime estimation in LIB fusion applications.

Speculative Approach

In addition to the conventional design approach, a more speculative idea that may aid in the integration of LIB fusion into a reactor system has been investigated. This idea involves the creation of an asymmetric blast wave in the reactor cavity by tailoring the density or opacity of the gas. This is shown schematically in Fig.I-6. If a density gradient can be established in the cavity gas, then the blast wave resulting from the micro-explosion will "vent" down the density gradient. The cavity can be shaped as a long cylinder allowing the diodes to be brought closer to the target without increasing the overpressure that they would experience. This might improve the beam transport efficiency or the channel formation process. Such a scheme might also be useful for a materials test facility where samples can be brought up close to the target without experiencing a severe overpressure. This non-symmetric blast idea appears to have promise but has not yet been studied to the extent that the conventional approach discussed earlier has been.

Reportage

This study of cavity and first wall design includes the analysis of different problems in diverse fields of engineering and physics. Each of

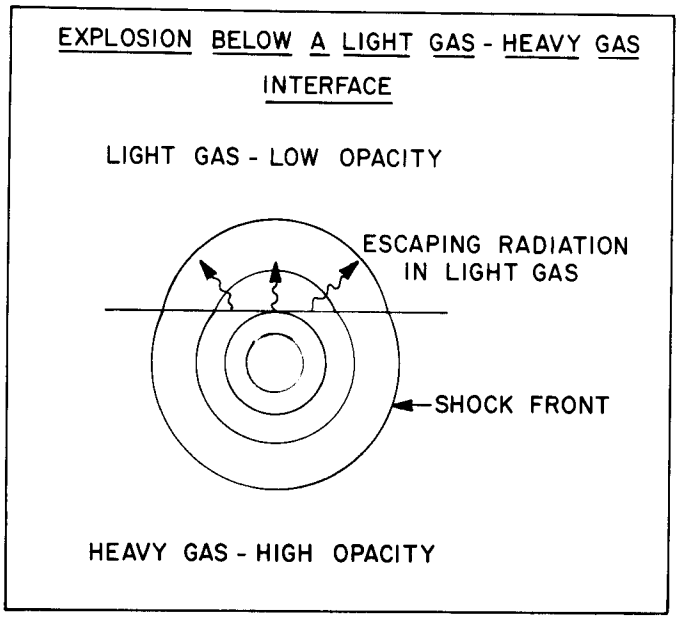
EXPLOSION BELOW A LIGHT GAS - HEAVY GAS INTERFACE
LIGHT GAS - LOW OPACITY
ESCAPING RADIATION IN LIGHT GAS
SHOCK FRONT
HEAVY GAS - HIGH OPACITY

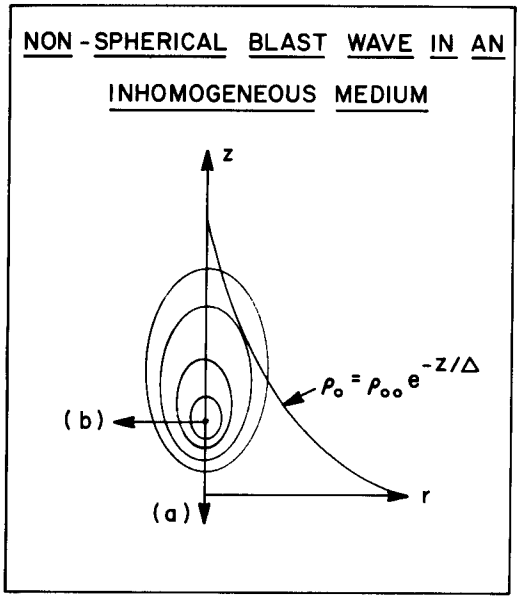
NON - SPHERICAL BLAST WAVE IN AN INHOMOGENEOUS MEDIUM
z
$\rho_o = \rho_{oo} e^{-z/\Delta}$
(b)
r
(a)

Fig. I-6

these analyses is reported separately in a UWFDM report. These reports are listed in Table I-4 along with their authors. The remainder of this report is a brief summary of each of these separate technical areas and the conclusions of the study. The conclusions are presented in Part II. The blast wave and fireball calculations are described in Part III. Parts IV and V are a discussion of mechanical and thermal response of the first wall. Part VI deals with the gas recirculation system and Part VII is a discussion of the neutronics and radiation damage analysis.

References for Part I

1. D.J. Johnson, et al., Phys. Rev. Lett. 42, 610 (1979).

2. Unpublished communication.

3. D.L. Cook and M.A. Sweeney, "Design of Compact Particle Beam Driven ICF Reactors," Proc. 3rd Topical Meeting on Technology of Controlled Nuclear Fusion, CONF-780508, ANS (1979).

Table I-4

List of UWFDM Reports Relating to the LIB Fusion Study

UWFDM #	Title	Authors
295	Pellet and Pellet Blanket Neutronics and Photonics for Electron Beam Fusion Micro-Explosions(1)	M. M. Ragheb, G. A. Moses, C. W. Maynard
300	Compact Electron Beam or Light Ion Beam Fusion Reactor Cavity Design Using Non-Spherical Blast Waves(2)	G. A. Moses, R. Spencer
307	MFP - A Calculation of Radiation Mean Free Paths, Ionization and Internal Energies in Noble Gases(3)	R. R. Peterson, G. A. Moses
315	Blast Wave Calculations in Argon Cavity Gas for Light Ion Beam Fusion Reactors(4)	R. R. Peterson, G. A. Moses
322	LIB Fusion Reactor First Wall Mechanical Design(5)	E. Lovell, R. Engelstad
320	First Wall and Cavity Design Studies for a Light Ion Beam Driven Fusion Reactor(6)	

(1) Accepted for publication in Nuclear Technology.
(2) Accepted for publication in Nuclear Fusion.
(3) Submitted for publication in Computer Physics Communications.
(4) Submitted for publication along with calculations for gas protection in laser fusion reactors in Nuclear Fusion.
(5) Will be submitted for publication in Nuclear Technology.
(6) Will be submitted to the ANS 4th Topical Meeting on Fusion Technology.

II. Conclusions

The major conclusions of this LIB fusion reactor study are presented in this part. The technical basis upon which these conclusions are derived is summarized in the remainder of this report. Detailed accounts of the technical work are presented in separate UWFDM reports attached with this summary.

(1) Light ion beam fusion reactor first walls can be designed to accommodate the blast overpressure from the pellet explosion using standard engineering design techniques, conventional materials such as stainless steel, and very conservative engineering design factors. Realistic designs are possible using a stress limit of 5 times less than the yield strength, assuming a maximum overpressure on the wall of 2 times more than is predicted by computer hydrodynamics calculations. This represents a full order of magnitude in conservative design criteria. Furthermore, this result is for the simplest wall design from a fabrication point of view. Additional factors of two or three can be achieved by more complex fabrication options. This conclusion is most important because it allows for large margins of error in areas of uncertainty without jeopardizing the viability of the wall design. An example of this uncertainty are the pulsed irradiation damage effects on the wall.

(2) Re-radiation of energy to the first wall can be minimized with the proper choice of cavity gas. If this is done then the thermal response of the wall poses no problem in its design. Furthermore, the wall may be actively cooled and operated at low temperature without severely penalizing the thermal efficiency of the reactor. Low temperature operation of the wall could improve its radiation damage properties and extend its lifetime. In combination, conclusions (1) and (2) are a very positive result.

(3) The response of the cavity gas to the X-ray and ion energy deposited into it is very dependent on the gas type. Noble gases, such as argon, are highly transparent at $T < 1$ eV. The expanding fireball created by the microexplosion drops below the transparency temperature before its shock front reaches the wall. At this time the fireball radiates energy to the wall with a high instantaneous heat flux. This heat flux is unacceptably high for stainless steel walls. Hence the use of noble gases in the cavity is questionable if stainless steel walls are used and a minimum radius is desired. Molecular gases might not re-radiate their energy in such a burst of X-rays because they are less transparent at low temperatures. The stainless steel wall response to these gases will likely be acceptable.

(4) The cavity gas recirculation system poses some unanswered questions. To bring the average exit temperature of the cavity gas down to a value consistent with state-of-the-art heat exchanger equipment requires excessively high flow rates and compressor power. Conversely, if lower flow rates are used, then the gas temperature is too high. Furthermore, the pressure of the cavity gas is an order of magnitude lower than the pressures used in conventional heat transfer equipment. To allow the gas to exchange all of its energy with the first wall in a cyclic steady state requires an average gas temperature in the cavity of 8000-9000°K depending on the gas type. A possible solution to this problem is to allow the cavity gas to exit at a high temperature, but then mix this gas with a lower temperature, high pressure gas stream before introduction into the heat transfer equipment. This requires some development of very high temperature gas handling equipment, but has the advantage of isolating the problems to a small part of the overall recirculation system.

(5) Neutronics calculations that take account of the target material surrounding the burning DT fuel show that the radiation damage parameters (dpa, He and H production) are only reduced by about 20% due to the presence of down scattering and (n,2n) reactions in the pellet. Tritium breeding ratios in the blanket are about the same as for a pure 14.1 MeV source. Such a result indicates that the exact target characteristics are not necessarily important to the neutronics design of the blanket.

(6) Radiation damage to the first wall is of a pulsed nature. Indications are that the wall response to this damage will be different than in a steady state irradiation environment. Therefore first wall lifetimes cannot be realistically assessed at this time. However, the conservatism in the wall design discussed earlier adds an element of optimism with regard to this very important uncertainty. Such radiation damage uncertainties are true for all inertial confinement reactor designs to date. Many designs cannot claim the conservatism of this one.

(7) A novel cavity design has been proposed to utilize the behavior of point explosions in a non-uniform density background gas. Under the proper conditions, the blast wave from the point explosion might preferentially vent down the density gradient. If such a density gradient can be established in a direction that is perpendicular to the plane of the diodes in a LIB reactor, then the overpressure experienced at the diodes could be significantly reduced. This might also allow the diodes to be brought closer to the target, thus improving the beam transport efficiency. A reactor cavity based on this concept might be very appropriate for a materials test facility where samples can be brought close to the exploding target (in the direction of increasing gas density) without suffering damage from the blast.

These represent the major conclusions of this LIB fusion reactor study. Many more conclusions, of a more specific nature, are included in the detailed descriptions of the analysis.

III. Fireball Calculations

The light ion beam reactor cavity is filled with a buffer gas at a density of $3.5 \times 10^{17} - 3.5 \times 10^{18}$ cm^{-3}. This corresponds to a gas pressure of 10-100 torr at 0°C. This buffer gas serves as the medium in which ionized channels are created to propagate the ion beams from the diodes to the target.[1] Hence this buffer gas is an essential part of the driver-pellet coupling system. In addition to this essential function it also serves to protect the first wall of the reactor from the X-rays and ion debris that are released from the target during the thermonuclear microexplosion. In fact, X-ray and ion stopping calculations show that in 50 torr of moderate Z gas, the range of the most energetic X-rays and ions is only a few centimeters.[2] Hence the buffer gas, at those densities required for beam propagation through ionized channels, very effectively shields the wall from direct bombardment by target debris. However, stopping the target debris in such a small volume of gas creates a hot (50-100 eV) ball of plasma at the center of the cavity. This fireball expands outward, driving a strong shock ahead of it. This shock, along with the radiant heat flux from the fireball, ultimately impinges on the first wall. It is this mechanical and thermal load that the first wall must be designed to accommodate. It is therefore crucial to the first wall design that this overpressure and heat flux be calculated. In this part of the report, the fundamental issues regarding this problem will be outlined along with the computer model that is used for the calculations. This discussion is followed by some results of the

detailed calculations. The complete treatment of this part of the reactor study is reported in UWFDM-315.

In the remainder of this discussion it is assumed that the gas response to the exploding pellet can be treated as if one started with a ball of hot plasma 5-10 cm in radius, at the center of the cavity. The cavity gas response, subject to this initial condition, is modelled with a one-dimensional lagrangian hydrodynamics code named FIRE. This code treats the gas/plasma as a single fluid. However it allows for both a plasma temperature and a non-local equilibrium radiation temperature. With this two temperature model, the radiation can stream through the gas if its mean free path is long. This is very important for correctly modelling the dynamics of fireballs in noble gases such as argon. This code treats shock propagation using the standard technique of a von Neumann artificial viscosity. A very important element of this calculational model are the tabulated physical properties of the cavity buffer gas in the plasma state. The specific internal energy, charge state, Rosseland and Planck averaged radiation mean free paths are computed for noble gases using the MFP code (described in UWFDM-307). These quantities are computed using Saha equilibrium and semi-classical atomic models and are tabulated as functions of plasma density, plasma temperature, and radiation temperature. Examples of this data are shown in Fig. III-1 and III-2. The primary gas of interest in the calculations is argon. However, the properties of xenon are also available.

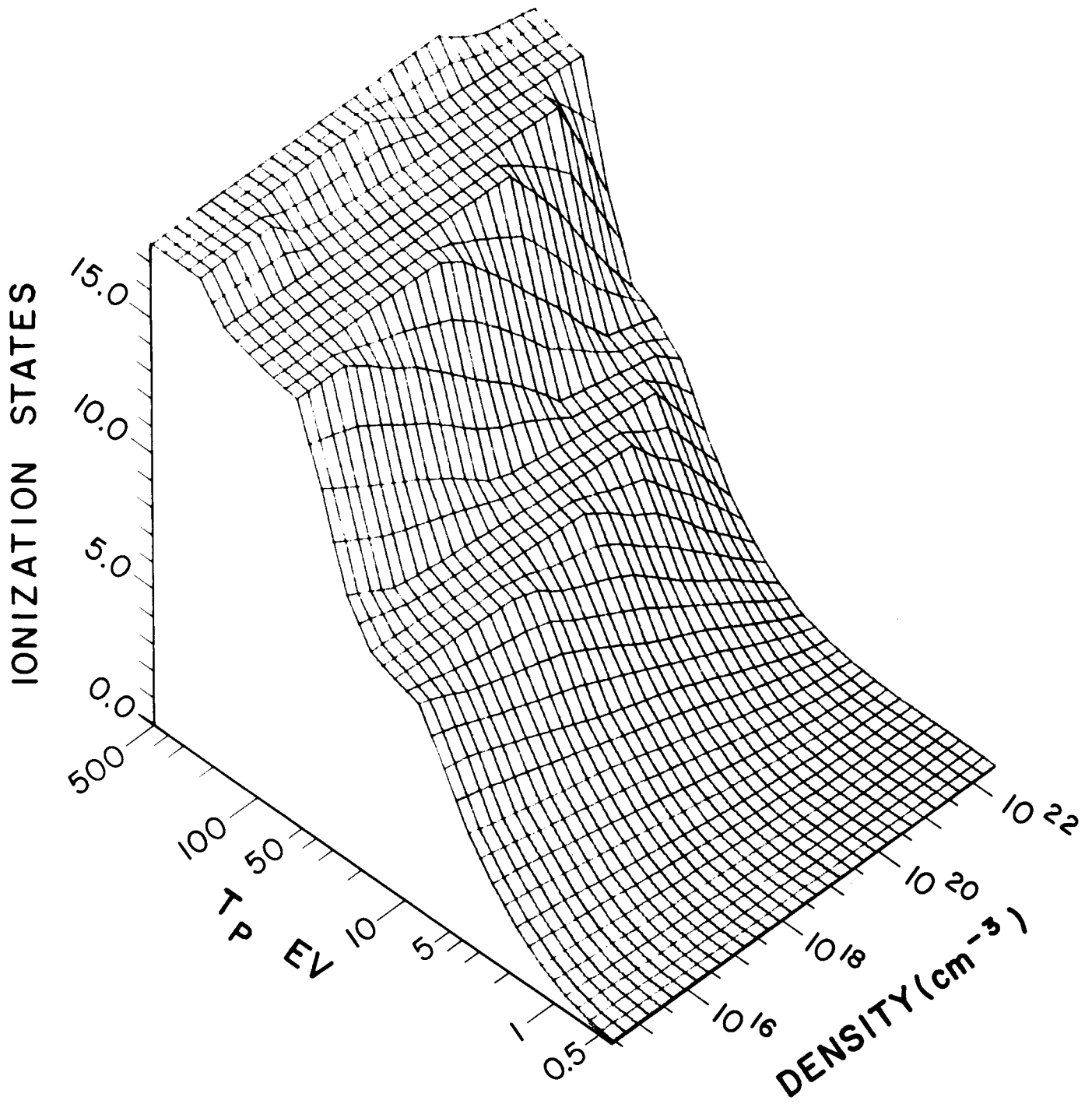

SAHA CHARGE STATE

ARGON

Fig. III-1

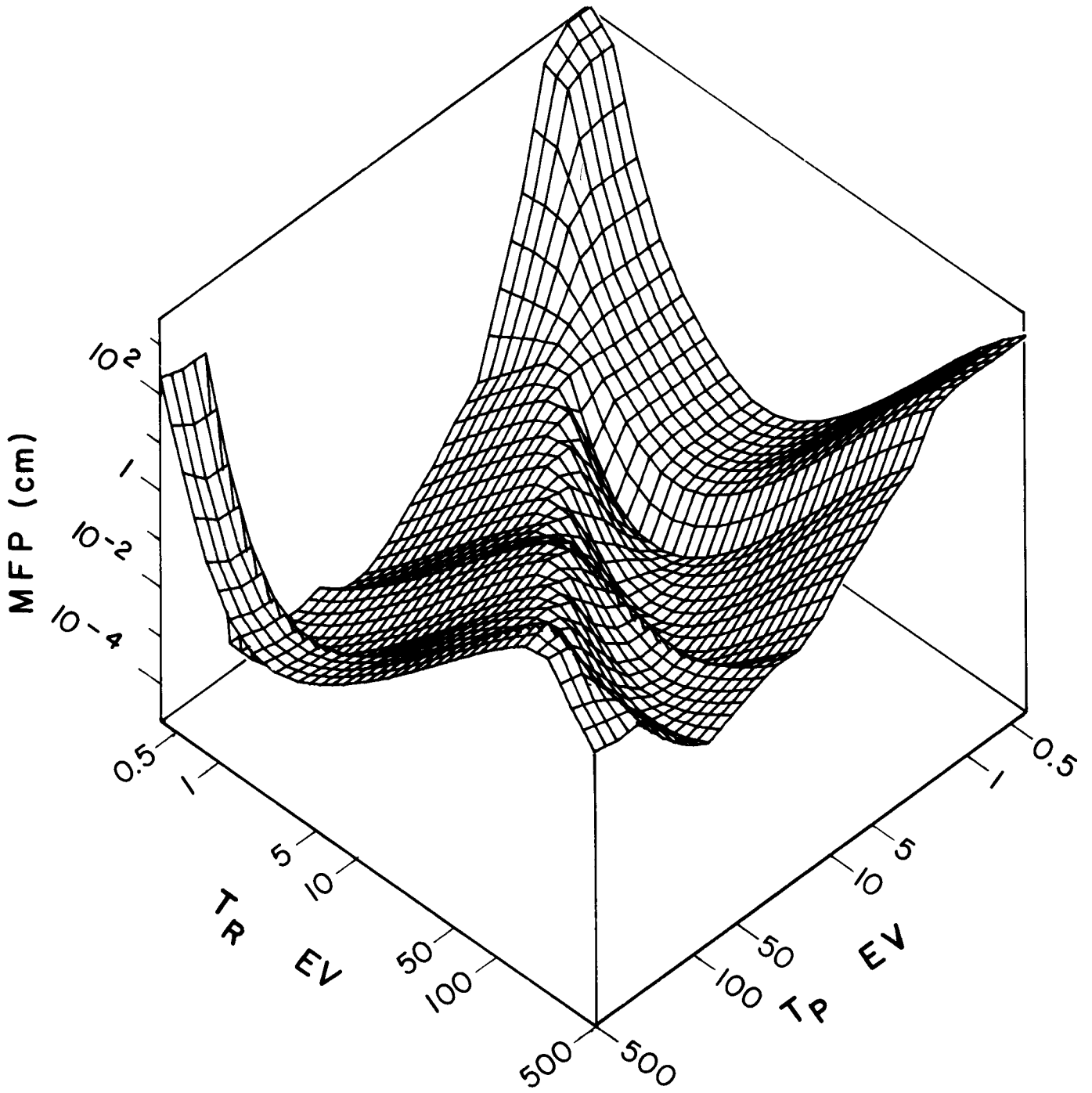
MFP (cm)
10 2
1
10 -2
10 -4
0.5
1
5
10
50
100
500
TR EV
0.5
1
5
10
50
100
500
TP EV
PLANCK MFP
ARGON DENSITY 2.7 x 10 19 cm -3

Fig. III-2

Fireball calculations are done for differing initial gas temperatures (0.05 eV, 0.1 eV, 0.5 eV, 0.7 eV, 1.0 eV). In each case a 10 cm hot plasma containing 30 MJ of energy is used as the initial condition. This plasma has a temperature of 64 eV. The resulting overpressures and heat radiated at the first wall for these calculations are shown in Table III-1. Note that more energy is radiated to the wall as the background gas temperature becomes hotter. Figures III-3 and III-4 show the shock propagation and the heat flux and overpressure as a function of time for the case of argon at an initial temperature of 1160°K (0.1 eV). Figure III-3 is an R-t plot of the plasma motion. The spherical plasma is divided into shells and the lines show the trajectories of these shells as the shock expands. Hence the position, R, of each shell is plotted as a function of time, t. The shock is clearly seen in this plot as the bunching of the lines. The line plotted along the shock trajectory is the result of a strong shock theory prediction of the shock position as a function of time. We see that agreement is not good between these two calculations. Hence, for the conditions under consideration here, the application of strong shock theory to compute the overpressure is not advisable. Figure III-4 shows the pressure and heat flux at the first wall as a function of time. The arrival time of the shock is at 2.3 msec after the explosion. The pressure pulse has a width (FWHM) of 1.2 msec. The shape of this pressure pulse is used to compute the dynamic load factor on the wall rather than simply assuming a value for this. This is discussed in more detail in UWFDM-322. The heat flux is nearly zero until 0.05 msec when it increases very rapidly and then decays away. This

Table III-1

Results of Fireball Calculations for Different Initial Gas Temperatures

Gas Temperature (°K)	Input Energy (MJ)	Energy Radiated to the First Wall (MJ)	Average Heat Flux (kW/cm^2)	Maximum Overpressure (Atm)
580	30	6.6	22	1.3
1160	30	7.5	15	1.5
5802	30	14.7	24	2.5
8123	30	20.3	29	2.75
11605	30	148	53	3.0

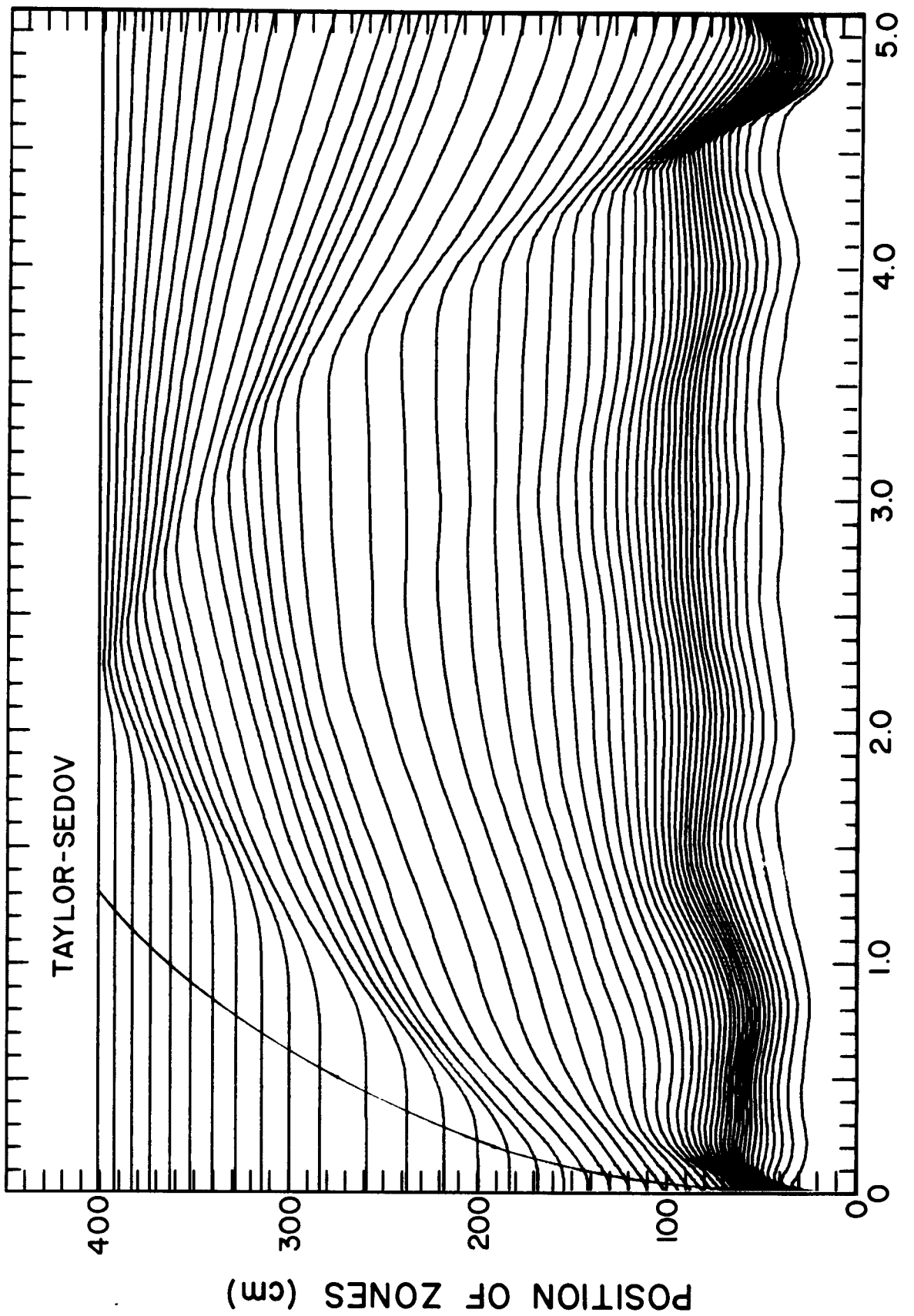
SHOCK PROPAGATION IN ARGON
T_{pcav} = 0.1 eV , N_p = 1.67x10^{18}cm^{-3} , E_{in} = 30 MJ
TAYLOR-SEDOV
POSITION OF ZONES (cm)
400
300
200
100
0
0
1.0
2.0
3.0
4.0
5.0
TIME (msec)

Fig. III-3

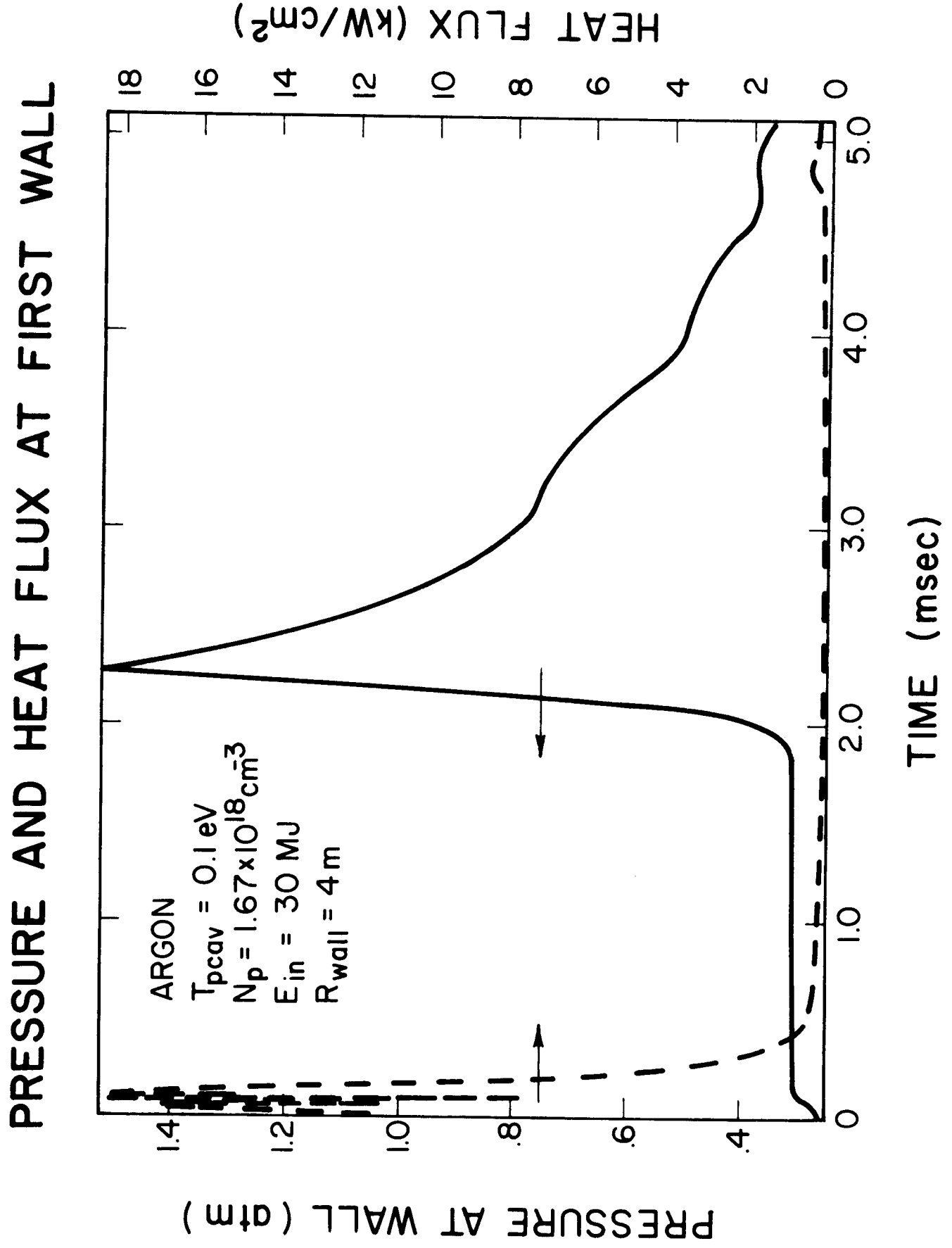
PRESSURE AND HEAT FLUX AT FIRST WALL
ARGON
T_{pcav} = 0.1 eV
N_p = 1.67x10^{18}cm^{-3}
E_{in} = 30 MJ
R_{wall} = 4 m
PRESSURE AT WALL (atm)
HEAT FLUX (kW/cm^2)
TIME (msec)
0
1.0
2.0
3.0
4.0
5.0
.4
.6
.8
1.0
1.2
1.4
0
2
4
6
8
10
12
14
16
18

Fig. III-4

phenomenon has been determined to be a consequence of using a noble gas as the cavity gas. This behavior can be explained by examining Fig. III-5 which shows the temperature profile of the cavity gas as a function of radius at different times during the fireball expansion. It is also useful to refer to Fig. III-6, a plot of the radiation mean free paths as a function of radiation temperature equal to plasma temperature. This is the condition of the plasma and radiation behind the shock front. At early times when the temperatures are high (>1 eV) the radiation mean free path behind the shock is short, hence no radiation leaks ahead of the shock. But as the fireball expands the temperature behind the shock falls until the temperature is low enough that the radiation mean free paths very rapidly become large compared to the fireball size. We see from Fig. III-5 that the plasma temperature falls to this level just at the time that the heat flux increases. Hence, the fireball expands until it becomes transparent to its own radiation and then it flashes this radiation to the wall, long before the shock arrives. The fireball almost instantaneously becomes a volume radiator rather than a surface radiator. The amount of energy leaked to the wall results in a wall temperature rise that cannot be tolerated for systems with a repetition rate of 10 Hz. This problem can be remedied in a variety of ways. (1) The cavity radius can be increased until the wall surface area is sufficiently large. (2) Another gas that is not monatomic can be used in the cavity. The monatomic nature of the noble gases leaves electronic transitions as the lowest energy mechanism for photon absorption. A polyatomic gas will

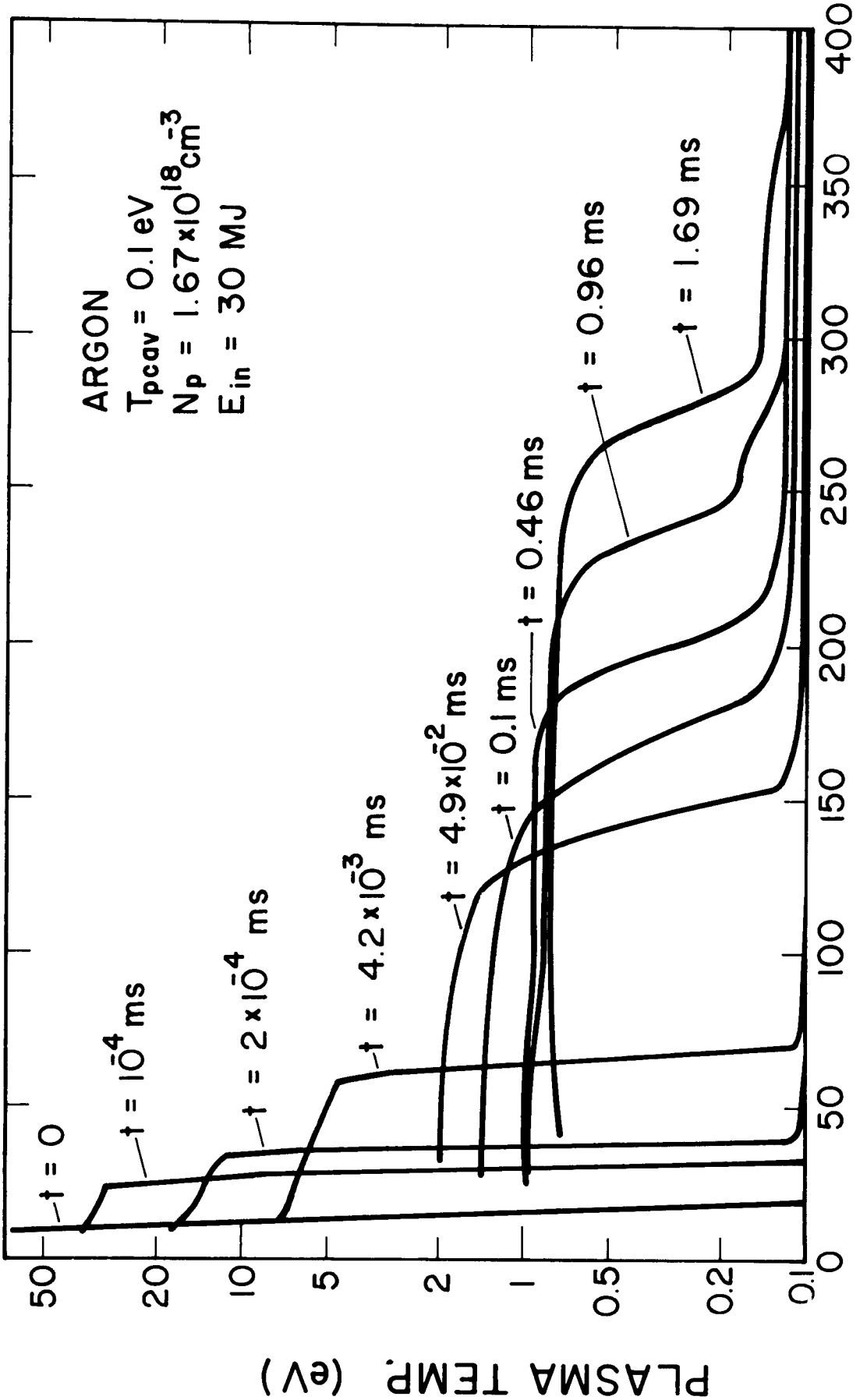
PLASMA TEMPERATURE
ARGON
T_{pcav} = 0.1 eV
N_p = 1.67x10^{18}cm^{-3}
E_{in} = 30 MJ
t = 0
t = 10^{-4} ms
t = 2x10^{-4} ms
t = 4.2x10^{-3} ms
t = 4.9x10^{-2} ms
t = 0.1 ms
t = 0.46 ms
t = 0.96 ms
t = 1.69 ms
PLASMA TEMP. (eV)
50
20
10
5
2
1
0.5
0.2
0.1
0
50
100
150
200
250
300
350
400
RADIUS (cm)

Fig. III-5

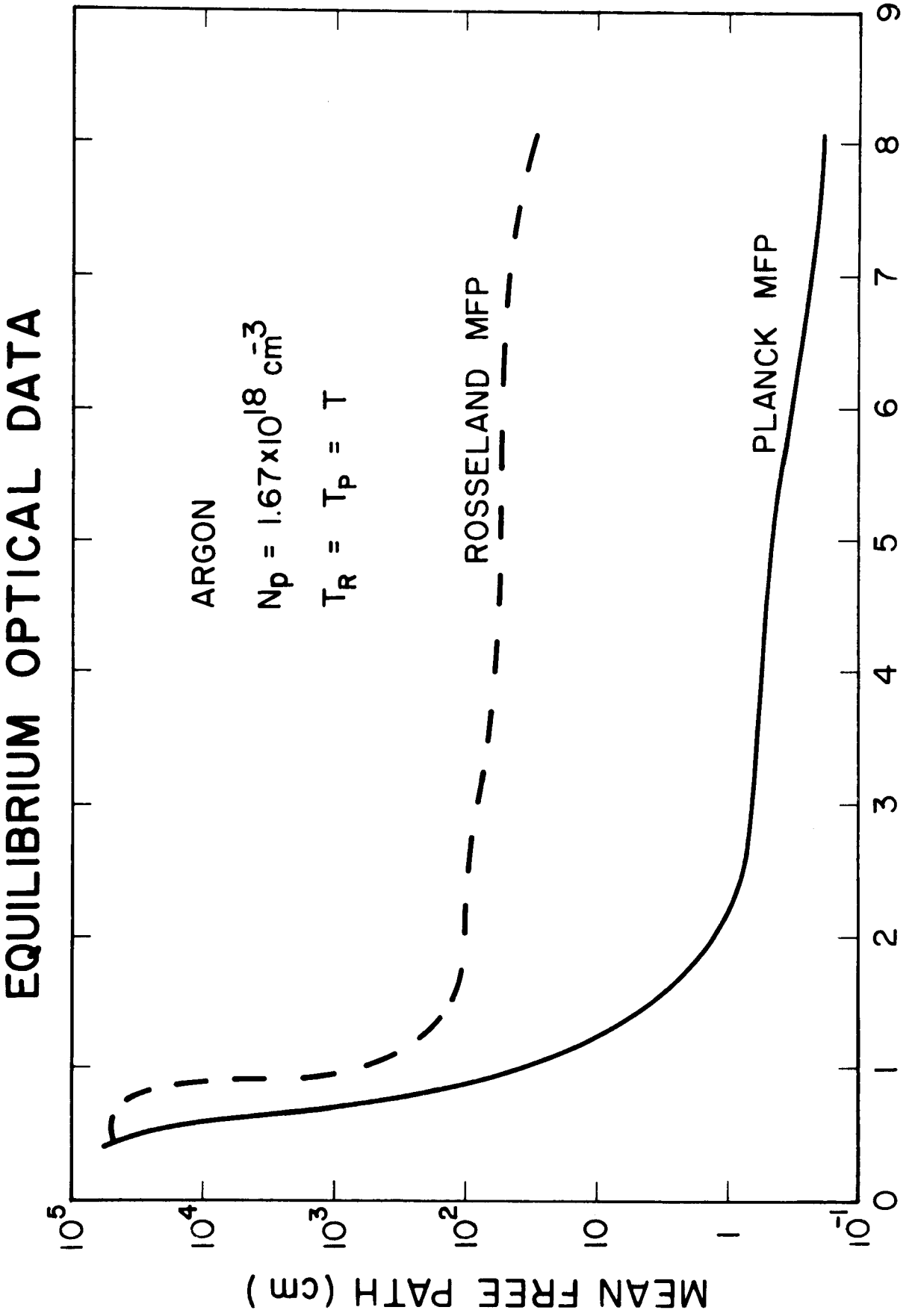
EQUILIBRIUM OPTICAL DATA
ARGON
$N_p = 1.67 \times 10^{18}\ cm^{-3}$
$T_R = T_p = T$
ROSSELAND MFP
PLANCK MFP
MEAN FREE PATH (cm)
10^5
10^4
10^3
10^2
10
1
10^{-1}
0
1
2
3
4
5
6
7
8
9
TEMPERATURE T (eV)

Fig. III-6

provide rotational and vibrational transitions that increase the opacity below the transparency temperature so that this leaking will not occur at any temperatures of interest in the reactor cavity. A gas such as nitrogen might be suitable. Such a phenomenon can be modelled by modifying the argon data to limit the radiation mean free paths below 1.5 eV. This new gas is called "diatomic argon"* for the purposes of this analysis. The results of the FIRE calculation for diatomic argon are shown in Fig. III-7. This figure confirms the explanation of the heat flux in Fig. III-4. In Fig. III-7 the heat flux remains low and only rises when the shock wave reaches the wall. In addition the maximum value of the heat flux is only 0.13 kW/cm^2 in this case whereas it is 18 kW/cm^2 in the case where the real argon data is used. In this latter case, only 0.15 MJ of energy is radiated to the wall. Fig. III-8 is an R-t plot for diatomic argon. It is clearly seen that in this case the shock propagation more closely follows the prediction of strong shock theory, as one would expect.

From these calculations it is obvious that the detailed properties of the cavity gas are very important to the fireball dynamics. The high transparency of pure noble gases at low temperature allows a significant amount of energy to leak from the fireball before the shock reaches the wall. Under some circumstances this will be desirable. For instance, if the cavity gas is not recirculated at a high rate, this will promote the cooling of the gas between shots, hence the quasi-steady-state temperature of the gas may be lowered. In this study, the design goal is to minimize

*The "diatomic argon" was modelled using the argon data generated by the MFP code but with the restriction that the radiation mean free path not go above 50 cm even when the gas cools below its transparency temperature.

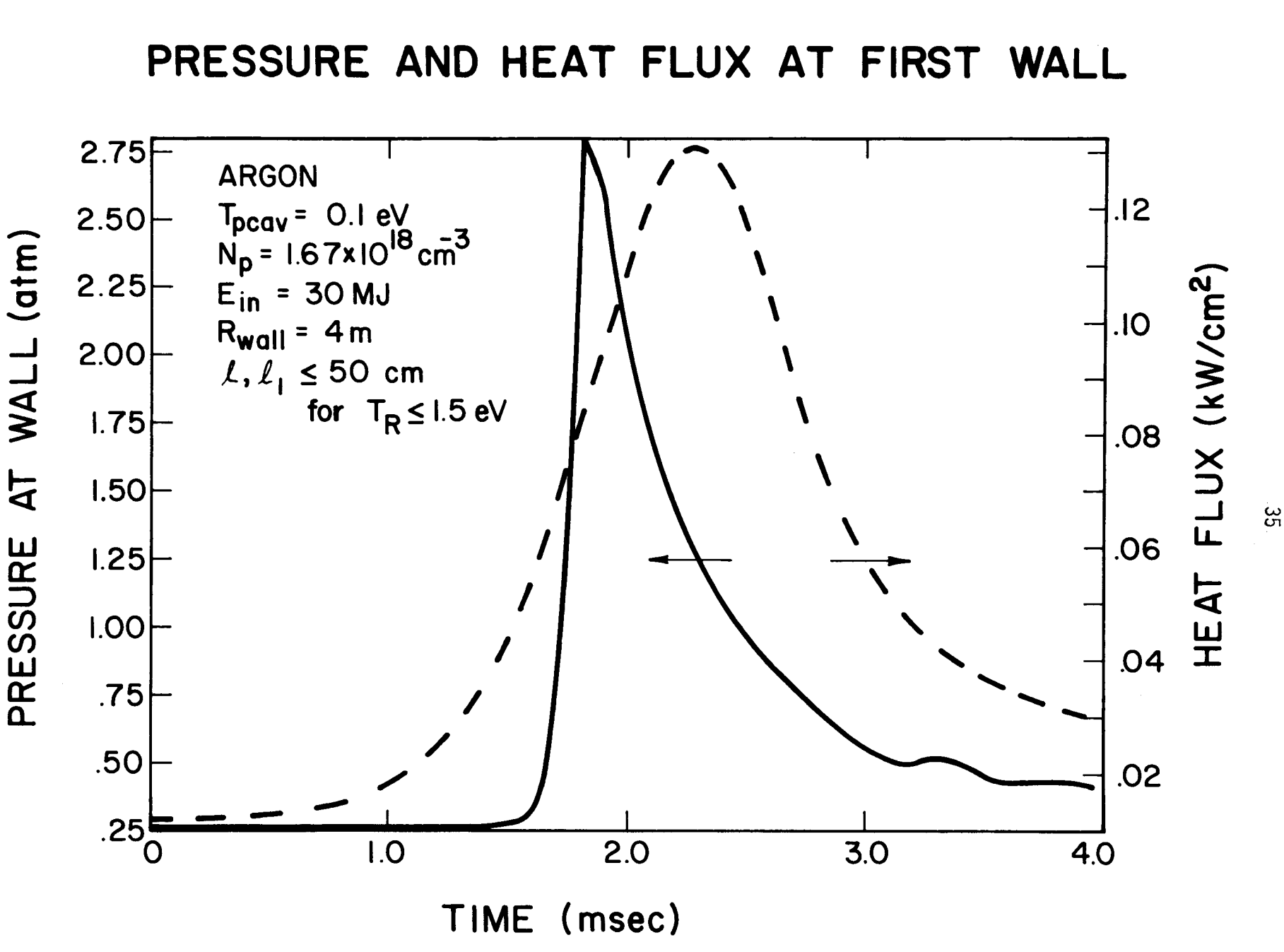
PRESSURE AND HEAT FLUX AT FIRST WALL
ARGON
T_{pcav} = 0.1 eV
$N_p = 1.67 \times 10^{18}$ cm^{-3}
E_{in} = 30 MJ
R_{wall} = 4 m
$\ell, \ell_1 \leq 50$ cm
for $T_R \leq 1.5$ eV
PRESSURE AT WALL (atm)
HEAT FLUX (kW/cm^2)
TIME (msec)
2.75
2.50
2.25
2.00
1.75
1.50
1.25
1.00
.75
.50
.25
.12
.10
.08
.06
.04
.02
0
1.0
2.0
3.0
4.0

Fig. III-7

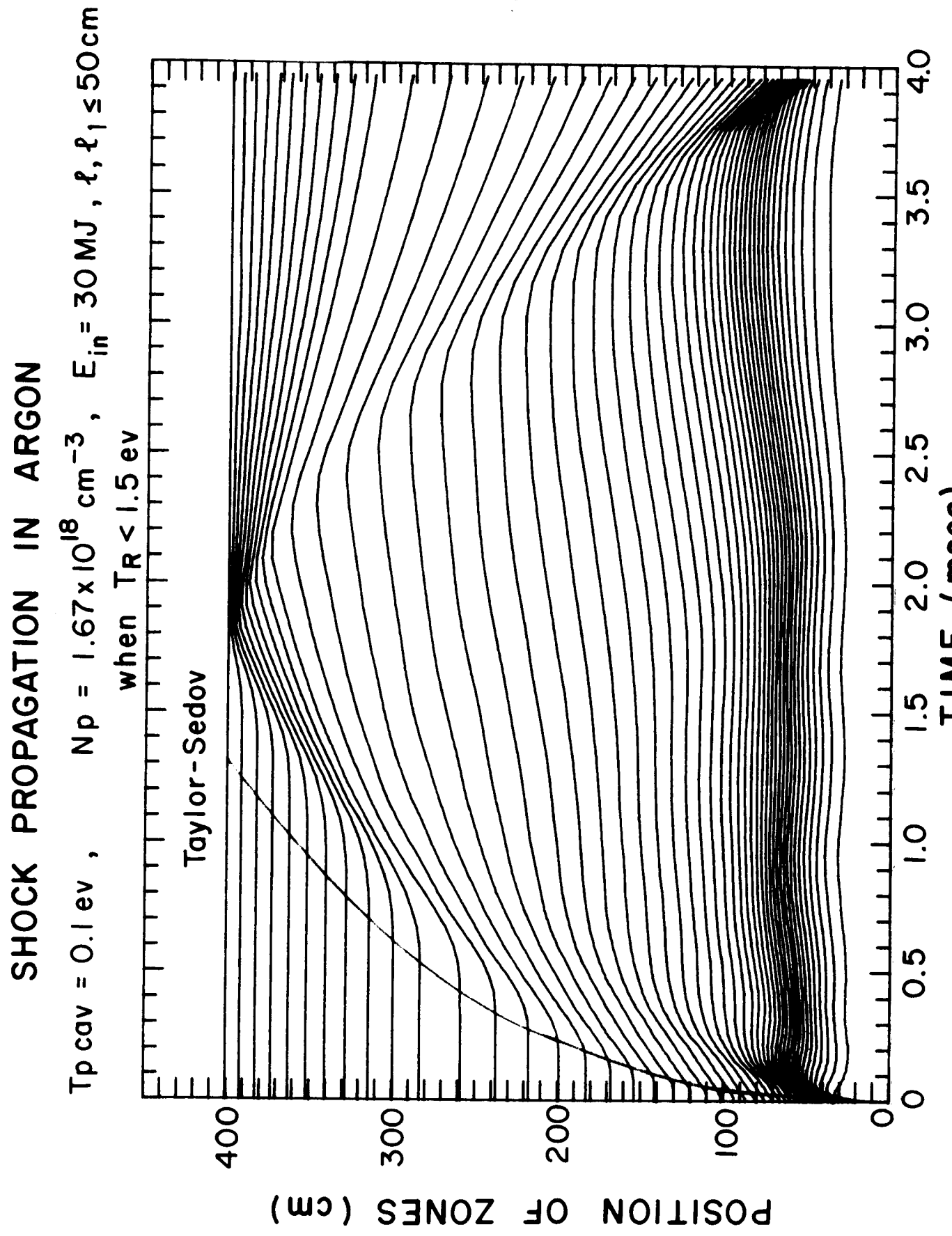
SHOCK PROPAGATION IN ARGON
Tp cav = 0.1 ev , Np = 1.67x10^18 cm^-3 , E_in = 30 MJ , ℓ, ℓ_1 ≤ 50 cm
when T_R < 1.5 ev
Taylor-Sedov
POSITION OF ZONES (cm)
TIME (msec)
0
100
200
300
400
0
0.5
1.0
1.5
2.0
2.5
3.0
3.5
4.0

Fig. III-8

the heat flux as much as possible so that the first wall can be designed to accommodate the mechanical load of the shock with as few constraints as possible. A gas with short radiation mean free paths down to low temperatures is desirable for this design and this implies the use of a molecular gas.

References for Part III

1. D. L. Cook, M. A. Sweeney, "Design of Compact Particle-Beam-Driven Inertial Confinement Fusion Reactors", Proc. 3rd Topical Meeting on Technology of Controlled Nuclear Fusion, CONF-780508, ANS, Santa Fe, NM (1979).

2. T. McCarville, private communication.

IV. First Wall Design and Mechanical Response

The first wall in a LIB fusion reactor must be designed to withstand a significant dynamic overpressure on a repetitive basis. Analyses in the past have treated the first wall as a spherical shell subject to a hoop stress when the load from the blast wave is applied.[1,2] In this study, a more "engineering oriented" design of the first wall is undertaken. A schematic diagram of this wall design is shown in Fig. IV-1. The wall itself may be constructed of panels or a continuous sheet that is reinforced from behind by a strong frame. This frame can then be joined to the back shield by supports to provide a very robust structure. The analysis of the first wall response to the overpressure is simplified by considering the flexural response of only one panel along with the appropriate boundary conditions for that panel. This analysis has been done. The panel itself need not be a solid panel. It could be a cellular plate as shown in Fig. IV-1. This adds stiffness to the plate without adding weight and the channels in the plate can be used for the purposes of active cooling. A detailed account of the first wall analysis is given in UWFDM-322. Here we provide a brief descriptive summary of this analysis and example wall designs.

Each panel is modelled as a flat plate rather than a curved plate. This is a good approximation so long as the ratio of plate thickness to radius of curvature is small. For the plate to be a section of a hemisphere, as shown in Fig. IV-1, it will not be rectangular in shape. However, it is shown in UWFDM-322 that it is acceptable to approximate a trapezoid as a rectangle so long as the ratio of height to span is greater than two. This

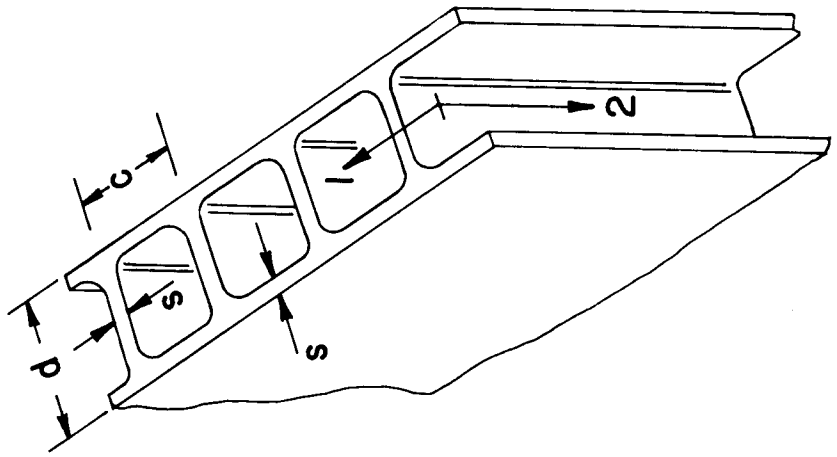

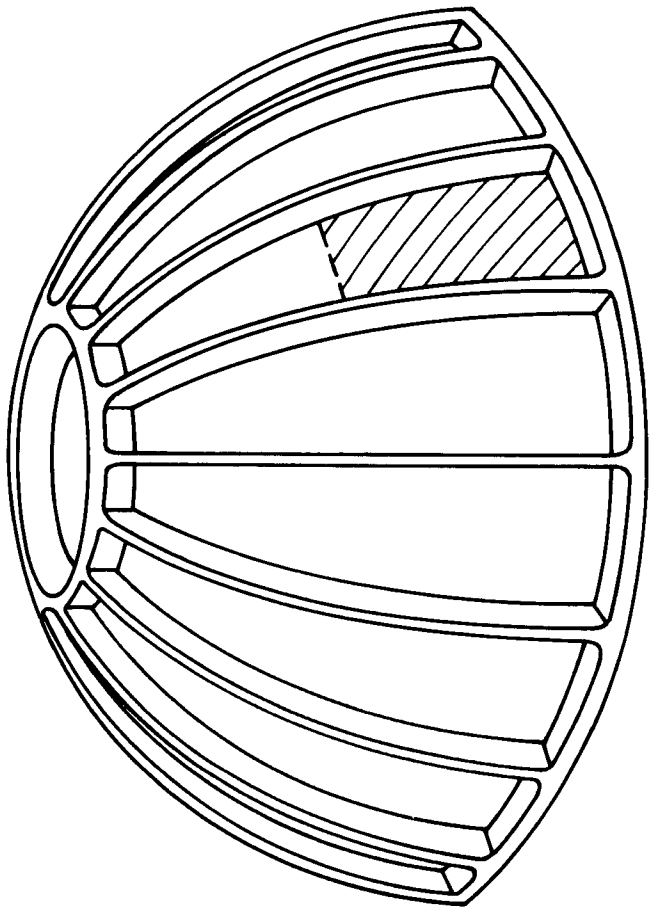

Fig. IV-1

is normally the case in this design. The equation of motion for this plate is solved using a modal analysis subject to appropriate boundary conditions. These boundary conditions are of two forms for a simply supported plate and a partially clamped plate. These are shown in Fig. IV-2. The solution to the equation of motion yields the maximum stress on the plate along with the maximum deflection and the frequency of vibration as a function of the plate dimensions. The results of these calculations for a stainless steel, cellular, simply supported plate are given in Figs. IV-3 to IV-5. The same quantities are displayed in Figs. IV-6 to IV-8 for a partially clamped plate. The difference between a solid plate and cellular plate only comes in the definition of the stiffness coefficient used in the analysis. Calculations of these same quantities are also done for a solid plate. Furthermore, these have all been done for both stainless steel and zircaloy as the wall material. Zircaloy is chosen because it has far better thermal stress properties than stainless steel. The issues of the wall thermal response will be presented in Part V of this summary report.

The information in Figs. IV-3 to IV-8 can be used to design first wall panels. Table IV-1 is a list of combinations of parameters that limit the maximum stress to 20 ksi in stainless steel when the maximum overpressure is 4 atmospheres (or 58.9 psi). This overpressure is chosen to represent a maximum that might be expected from a 100 MJ explosion; 30 MJ fireball in a 50 torr gas enclosed in a 4 meter cavity. The maximum stress limit of 20 ksi is a factor of 2.5 below the yield strength of stainless steel, 50 ksi. This represents a conservative stress limit for unirradiated materials. However, upon irradiation this may change and no good estimate can be made at this

SIMPLY SUPPORTED AND CLAMPED PLATES

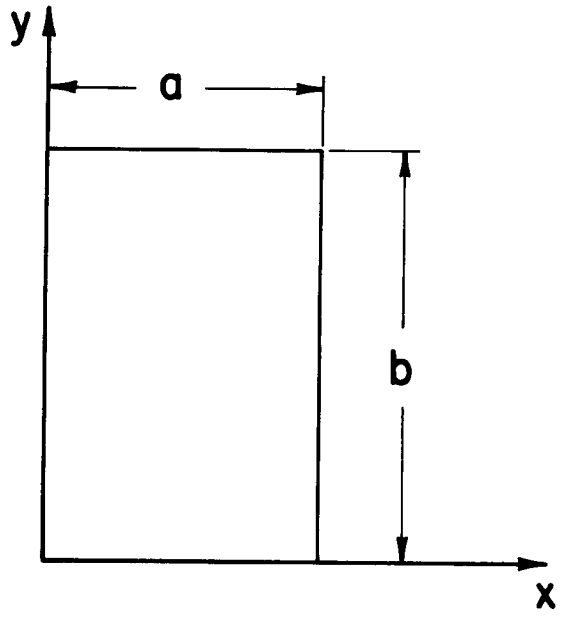

W(x,y) - DEFLECTION OF THE PLATE

SIMPLY SUPPORTED PLATE

$$\frac{\partial W}{\partial x}(0,y) = \frac{\partial W}{\partial x}(a,y) = \frac{\partial W}{\partial y}(x,0) = \frac{\partial W}{\partial y}(x,b) = 0$$

PARTIALLY CLAMPED PLATE

$$\frac{\partial W}{\partial y}(x,0) = \frac{\partial W}{\partial y}(x,b) = 0\,, \quad W(0,y) = W(a,y) = 0$$

Fig. IV-2

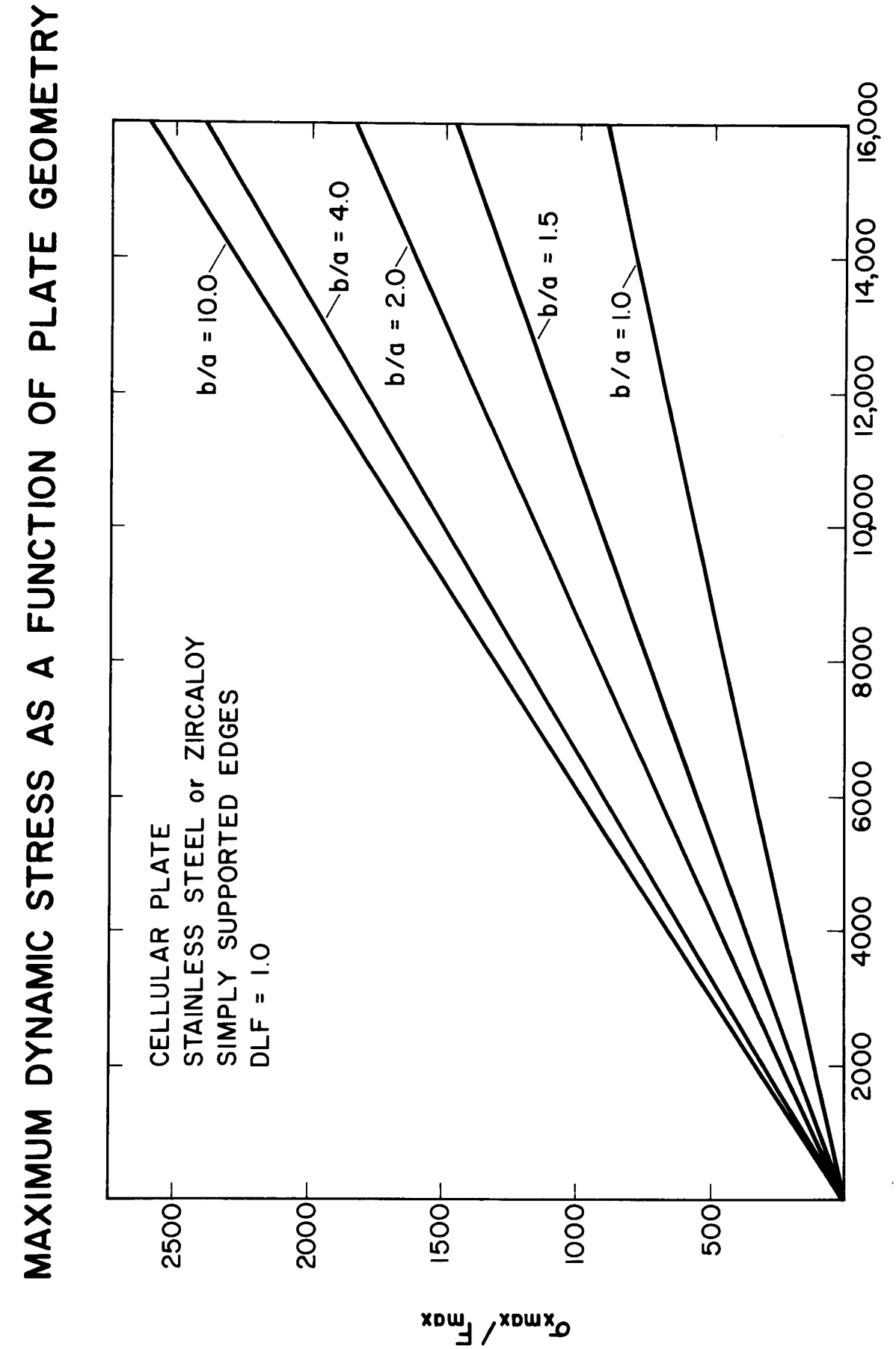
MAXIMUM DYNAMIC STRESS AS A FUNCTION OF PLATE GEOMETRY
CELLULAR PLATE
STAINLESS STEEL or ZIRCALOY
SIMPLY SUPPORTED EDGES
DLF = 1.0
b/a = 10.0
b/a = 4.0
b/a = 2.0
b/a = 1.5
b/a = 1.0
q_{xmax} / F_{max}
2500
2000
1500
1000
500
2000
4000
6000
8000
10,000
12,000
14,000
16,000
a^2/td

Fig. IV-3

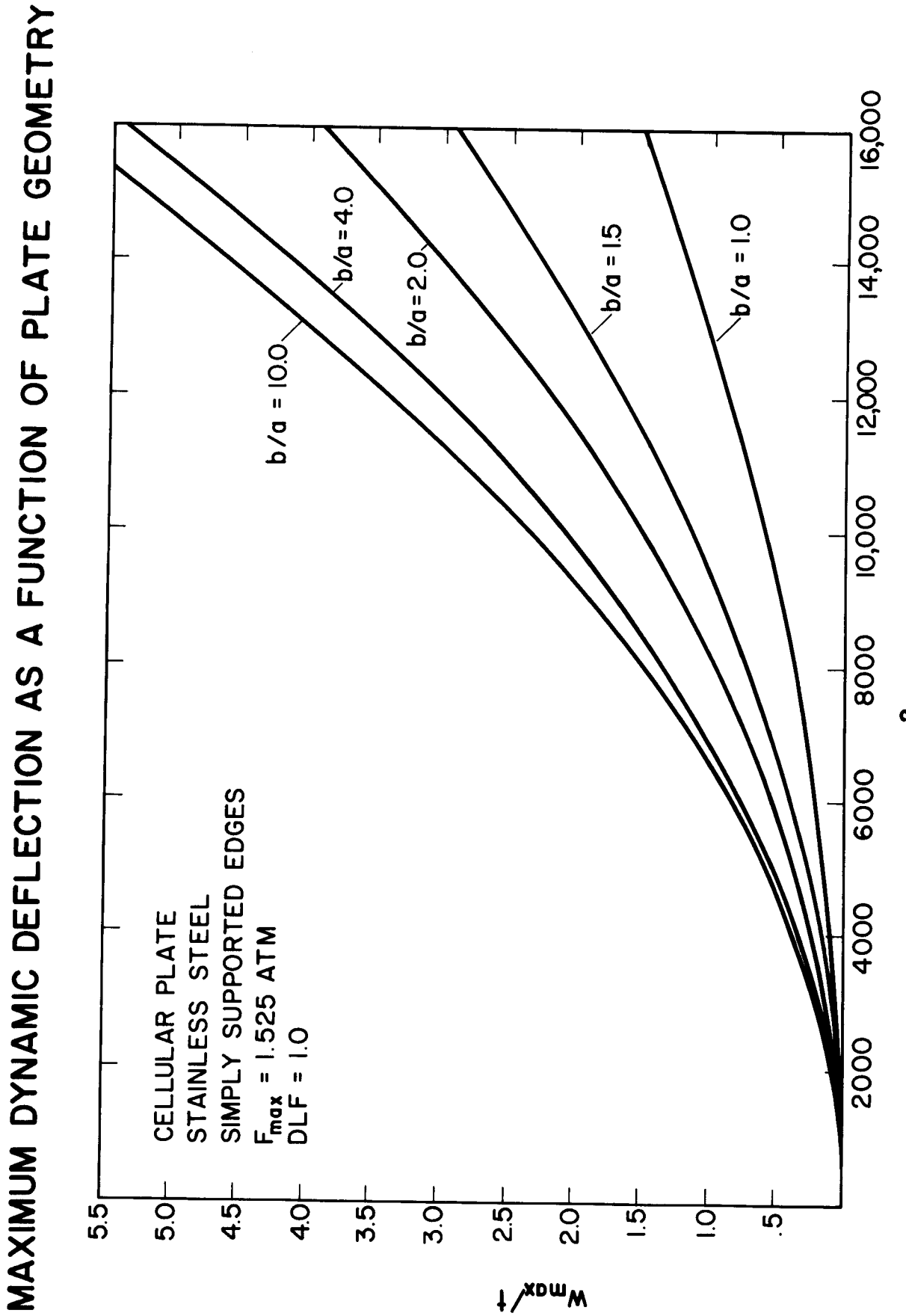
MAXIMUM DYNAMIC DEFLECTION AS A FUNCTION OF PLATE GEOMETRY
CELLULAR PLATE
STAINLESS STEEL
SIMPLY SUPPORTED EDGES
F_{max} = 1.525 ATM
DLF = 1.0
b/a = 10.0
b/a = 4.0
b/a = 2.0
b/a = 1.5
b/a = 1.0
W_{MAX}/t
a^2/td
5.5
5.0
4.5
4.0
3.5
3.0
2.5
2.0
1.5
1.0
.5
2000
4000
6000
8000
10,000
12,000
14,000
16,000

Fig. IV-4

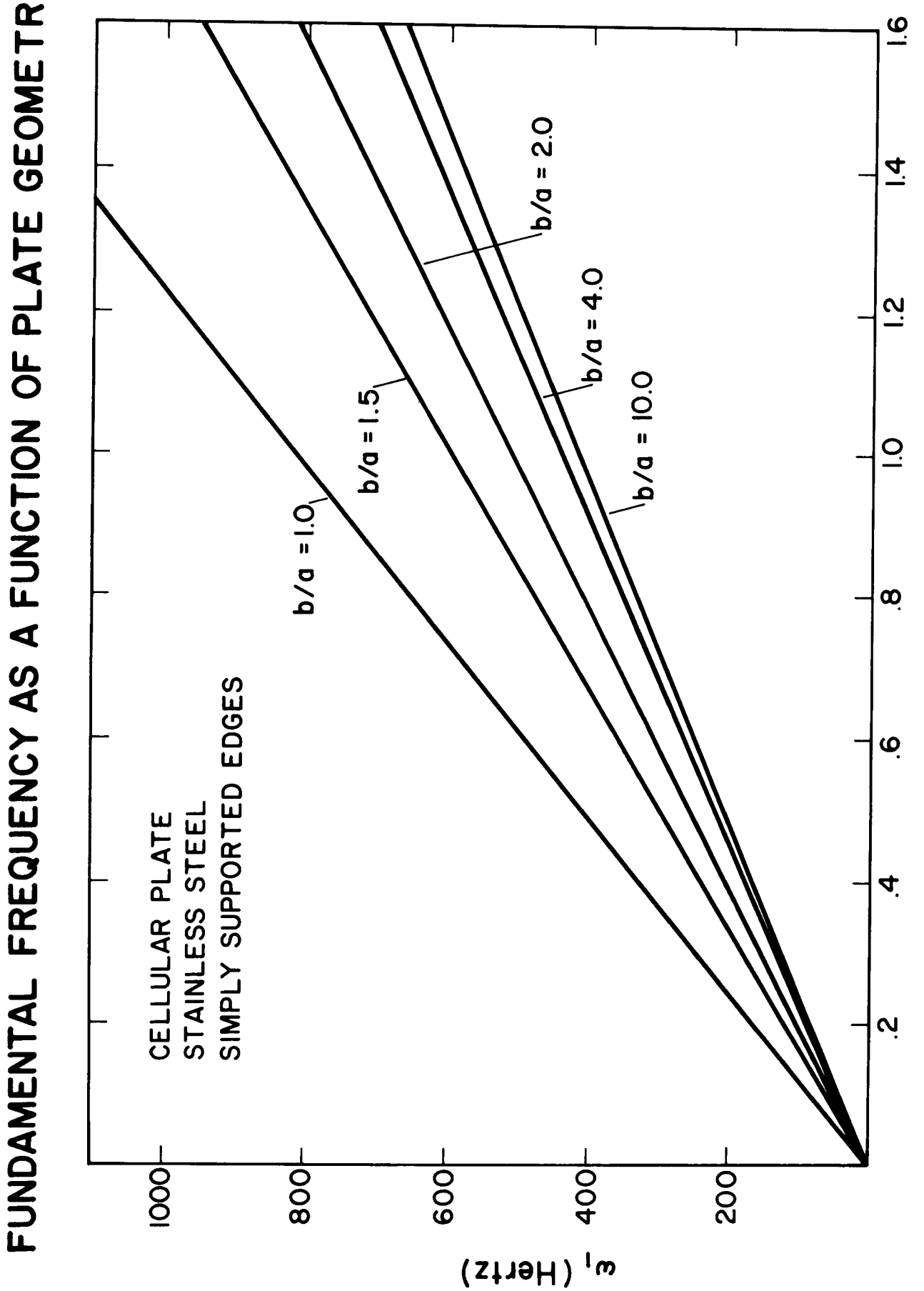
FUNDAMENTAL FREQUENCY AS A FUNCTION OF PLATE GEOMETRY
CELLULAR PLATE
STAINLESS STEEL
SIMPLY SUPPORTED EDGES
b/a = 1.0
b/a = 1.5
b/a = 2.0
b/a = 4.0
b/a = 10.0
ω1 (Hertz)
1000
800
600
400
200
.2
.4
.6
.8
1.0
1.2
1.4
1.6
d/a² (cm⁻¹ x 10⁻³)

Fig. IV-5

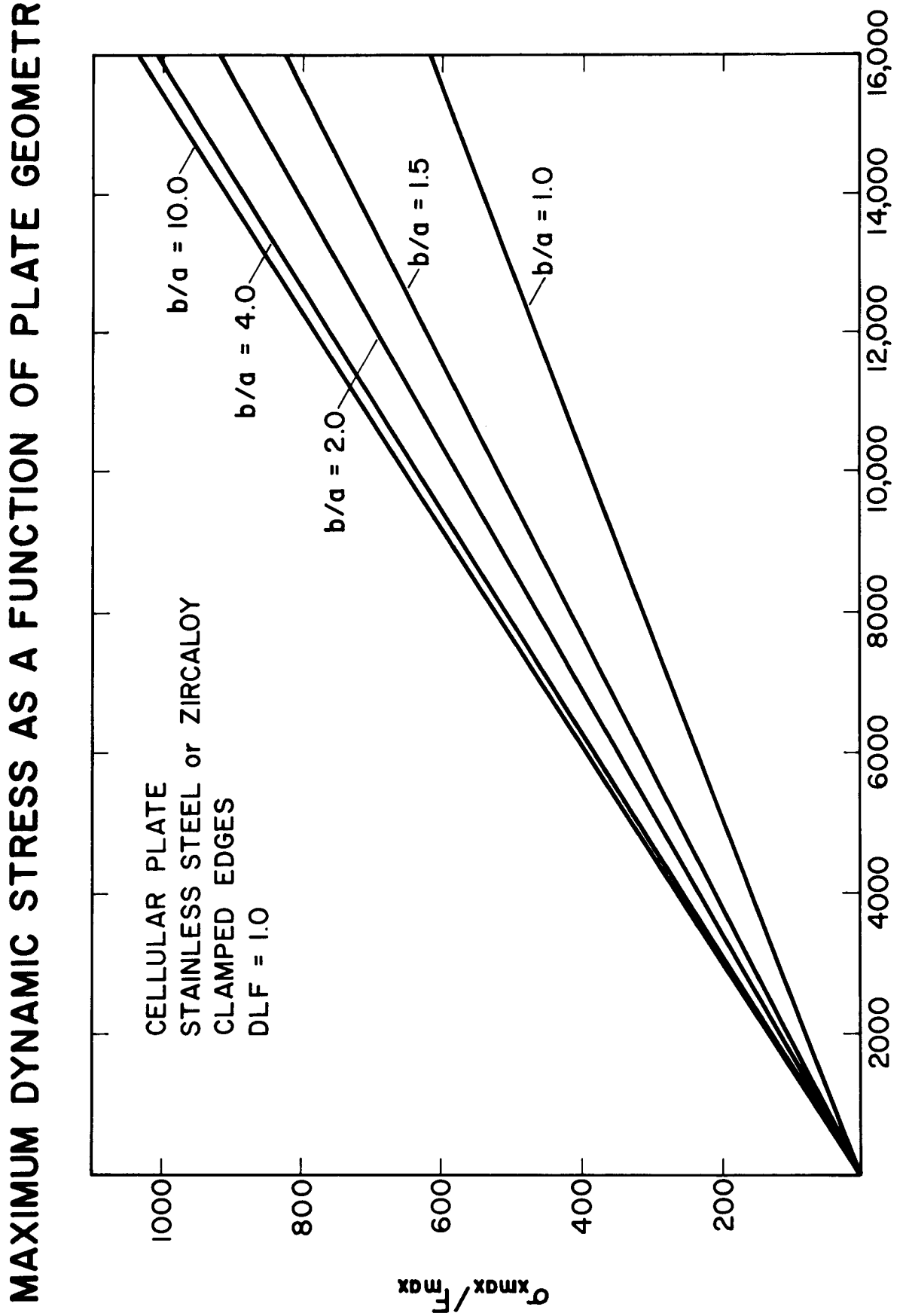
MAXIMUM DYNAMIC STRESS AS A FUNCTION OF PLATE GEOMETRY
CELLULAR PLATE
STAINLESS STEEL or ZIRCALOY
CLAMPED EDGES
DLF = 1.0
b/a = 10.0
b/a = 4.0
b/a = 2.0
b/a = 1.5
b/a = 1.0
$\sigma_{xmax}/\Gamma_{max}$
a^2/td
200
400
600
800
1000
2000
4000
6000
8000
10,000
12,000
14,000
16,000

Fig. IV-6

MAXIMUM DYNAMIC DEFLECTION AS A FUNCTION OF PLATE GEOMETRY

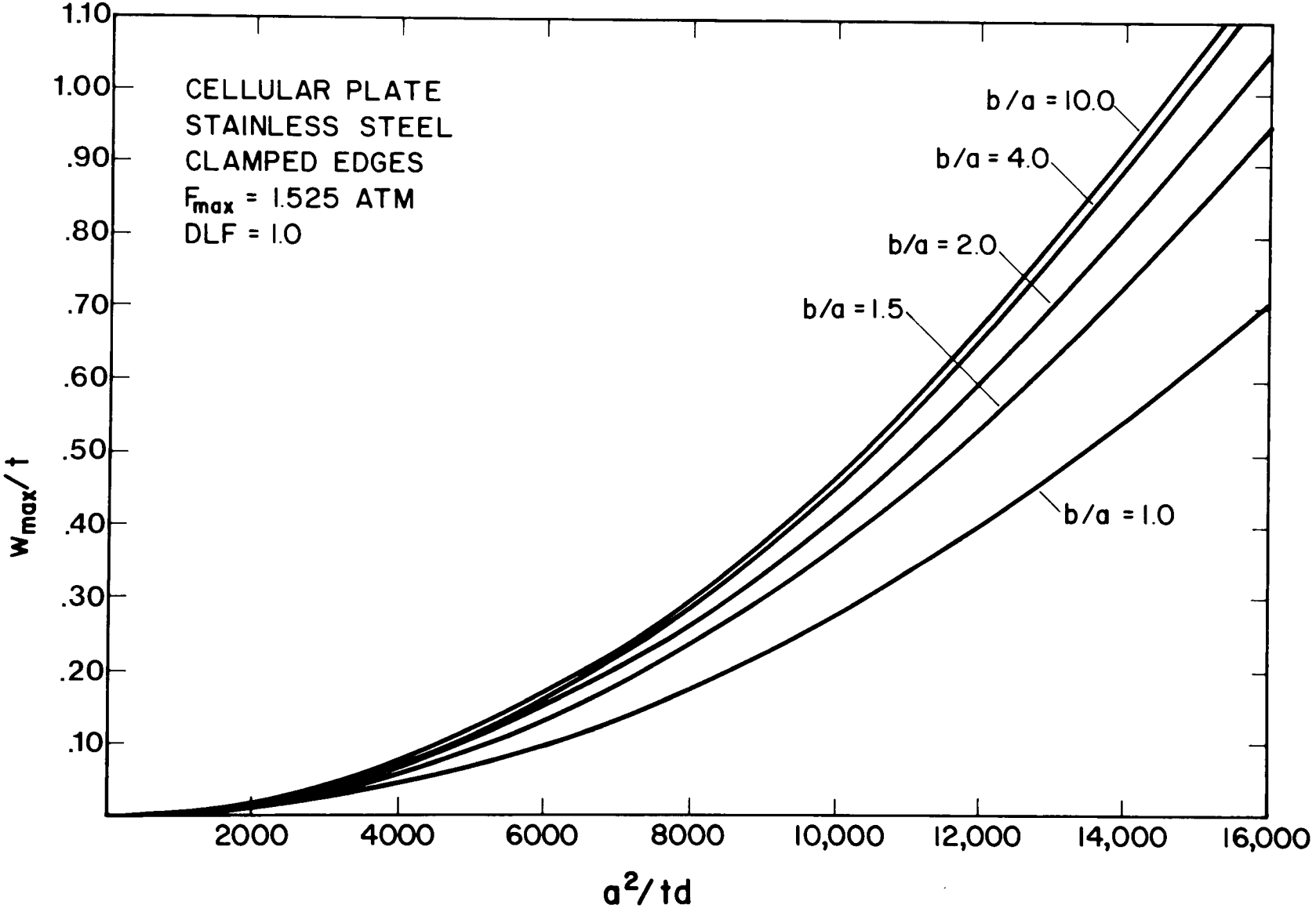

Fig. IV-7

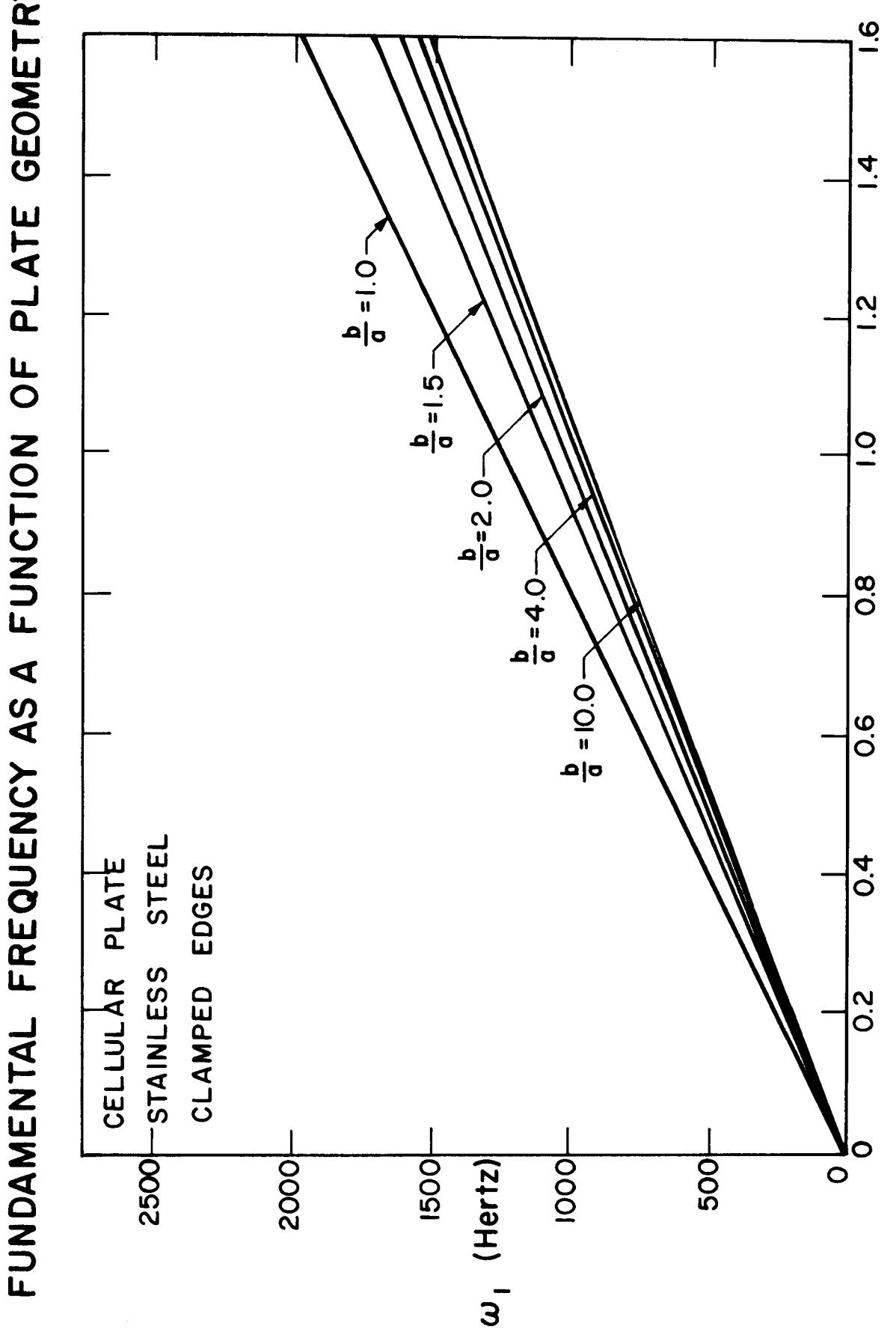
FUNDAMENTAL FREQUENCY AS A FUNCTION OF PLATE GEOMETRY
CELLULAR PLATE
STAINLESS STEEL
CLAMPED EDGES
$\frac{b}{a}$=1.0
$\frac{b}{a}$=1.5
$\frac{b}{a}$=2.0
$\frac{b}{a}$=4.0
$\frac{b}{a}$=10.0
ω_1 (Hertz)
2500
2000
1500
1000
500
0
0
0.2
0.4
0.6
0.8
1.0
1.2
1.4
1.6
d/a^2 ($cm^{-1} \times 10^{-3}$)

Fig. IV-8

Table IV-1

Design Parameters for First Wall with 20 ksi Stress Limit

Cavity Radius = 400 cm

Circumference = 2513.27 cm

Gas Duct Radius = 170 cm

Plate Height b = 420 cm

Maximum Stress = 20 ksi

Maximum P_w = 4 atm = 58.784 psi

$\sigma_{max}/P_{w\ max}$ = 340

	# of Panels/ Hemisphere	b(cm)	a(cm)	b/a	a^2/td	t	d
(1)	8	420	314.16	1.34	4640	0.5	42.54
(2)	16		157.08	2.67	2880	0.5	17.13
(3)	32		78.54	5.35	2200	0.5	5.61
(4)	8		314.16	1.34	4640	0.75	28.36
(5)	16		157.08	2.67	2880	0.75	11.42
(6)	32		78.54	5.35	2200	0.75	3.74
(7)	8		314.16	1.34	4640	1.0	21.27
(8)	16		157.08	2.67	2880	1.0	8.57
(9)	32	420	78.54	5.35	2200	1.0	2.80

time. Our gas response calculations (Part III) show that the overpressure may actually be as much as a factor of two less than this. For these calculations, it is assumed that the panels are simply supported. This would allow the use of a continuous first wall so that clamping to the structural frame is not required. By comparing Figs. IV-3 to IV-5 with Figs. IV-6 to IV-8 it is clear that this is also a conservative assumption since the stress levels in the clamped plate are smaller than in the simply supported one for the same overpressure. Table IV-1 clearly shows that for a variety of parameters there is no problem in designing a structure to accommodate a 4 atmosphere overpressure. Cases #3, 6, and 9 look to be particularly attractive. In each of these cases, there are 32 panels around the circumference of the reactor. These are joined at the waist of the cavity and at the gas inlet and outlet ducts at the top and bottom of the cavity. Fig. IV-4 shows that the deflection of the wall will be very small and Fig. IV-5 indicates that the resonant frequency of the plate vibration is much greater than the pulse repetition frequency. Hence, no resonant phenomena are expected.

This plate analysis can be applied to whichever final design parameters are chosen. Table IV-1 is only meant as an example. For instance, calculations are presented in Table IV-2 for a 10 ksi maximum stress limit rather than the 20 ksi value used in this example. Again, we see that viable parameters can be obtained for this more conservative limit.

From this analysis we must conclude that the mechanical overpressure generated by the cavity gas in a LIB fusion reactor can be easily accommodated by first wall structural designs that follow standard engineering design practice and that use conventional materials. Although questions remain about

Table IV-2

Design Parameters for First Wall with 10 ksi Stress Limit

Cavity Radius = 400 cm

Circumference = 2513.27 cm

Gas Duct Radius = 170 cm

Plate Height (b) = 420 cm

Maximum Stress = 10 ksi

Maximum P_w = 58.8 psi

$\sigma_{max}/P_{w\ max}$ = 170

	# of Panels/ Hemisphere	b(cm)	a(cm)	b/a	a^2/td	t	d
(1)	32	420	78.54	5.35	1040	0.5	11.86
(2)	32	420	78.54	5.35	1040	0.75	7.91
(3)	32	420	78.54	5.35	1040	1.0	5.93

the effects of radiation damage we are encouraged by the conservatism that is allowed in these designs for typical reactor conditions.

References for Part IV

1. Ref. 1, Part III

2. I. O. Bohachevsky, "Scaling of Reactor Cavity Wall Loads and Stresses", LA-7014-MS, Nov. 1977.

V. First Wall Thermal Response

The first wall in a LIB fusion reactor experiences both a mechanical overpressure and radiant heat flux following the pellet microexplosion. The response of the wall to the mechanical overpressure is discussed in Part IV of this report with the conclusion that walls can be designed to withstand this overpressure. In this section we discuss the wall response to the radiant heat flux.

Large temperature rises will lead to unacceptably high thermal stresses. Hence it is important to know the time dependent thermal response of the wall to the pulse of radiant energy that strikes it. For purposes of computing this transient response, the wall is modelled as a slab with a fixed temperature, T_b, on its back side. To the front of the slab a time varying heat flux is applied and the time dependent temperature diffusion equation is solved subject to these two boundary conditions, Fig. V-1. This heat flux is applied to the wall in a cyclic fashion until a cyclic steady state condition is reached. This means that the first wall temperature rises and falls back to the same value after each successive heat pulse. This cyclic steady state temperature response has been computed analytically by Abdel-Khalik[1] using a series solution. However in this analysis the time dependent temperature diffusion equation is solved numerically using a standard Crank-Nicholson[2] finite difference technique. This allows great flexibility in the choice of the time dependent heat flux while giving both the transient response of the wall from a cold start and asymptotically approaching the cyclic steady state operating conditions. These conditions are normally reached after about 8-10 pulses. This computer code, WALL,

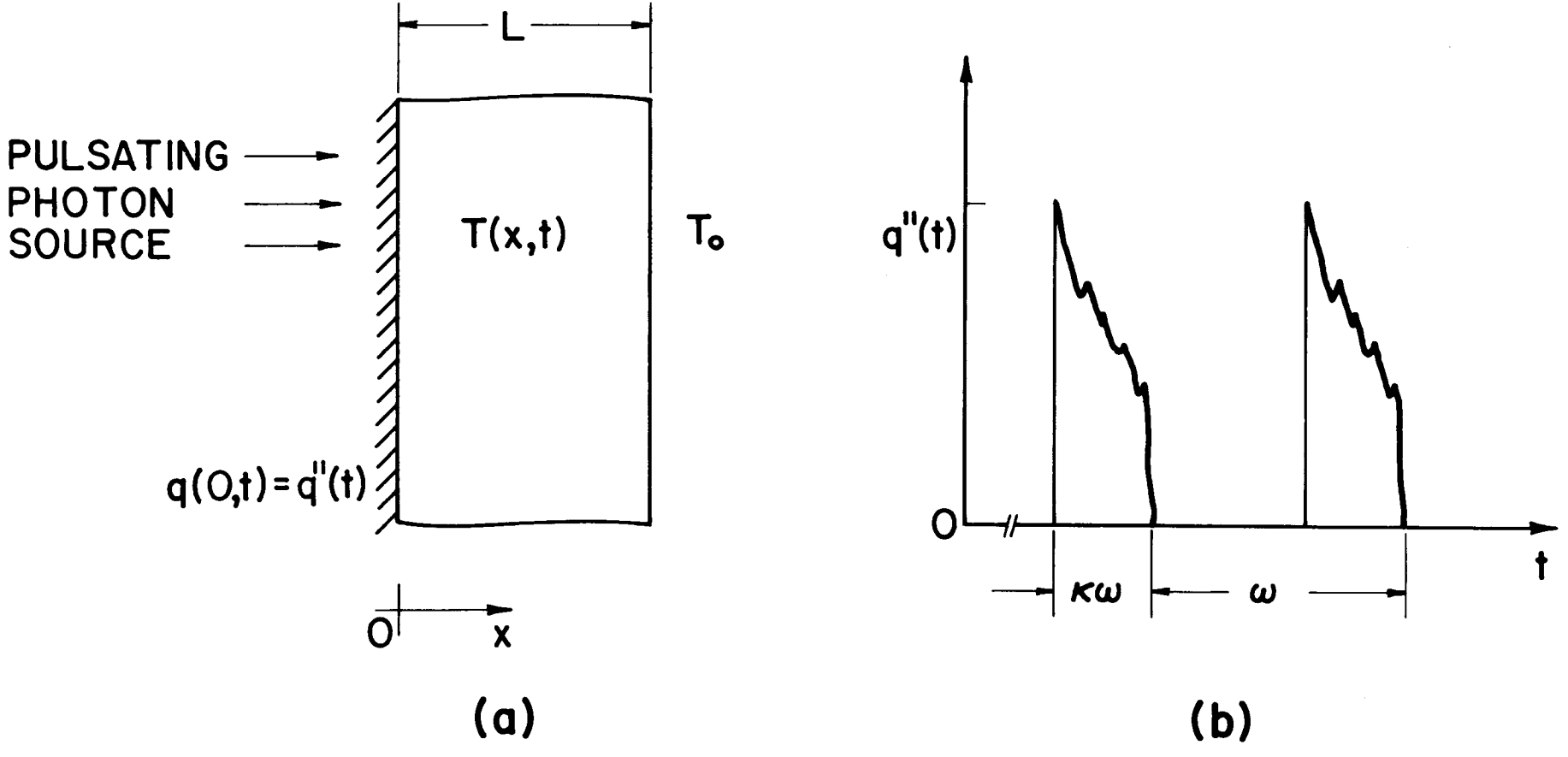

Fig. V-1

also conveniently couples to the output of the FIRE code so that no approximation need be made for the time dependence of the heat flux.

The wall response to a 30 MJ explosion in argon at 50 torr in a 4 meter cavity is shown in Fig. V-2. The cyclic steady state temperature difference between the front and back of the wall is shown as a function of time for a repetition rate of 10 Hz and 1 Hz.* This is for a 0.5 cm thick stainless steel wall. Three features in Fig. V-2 are most important. (1) There is a considerable difference between the 10 Hz and 1 Hz cases. The maximum temperature difference for the 10 Hz case is 20% larger than in the 1 Hz case, 317°C as compared to 266°C. Also the cyclic steady state temperature difference is 55°C for the 10 Hz case and only 5°C for the 1 Hz case. This demonstrates that the temperature response of the wall must be computed in the cyclic steady state limit with account taken for the repetition rate. (2) The temperature differences shown in Fig. V-2 are too high. These temperature differences lead to excessively high thermal stresses. This is a very important result. This means that noble gases such as argon may not be suitable as the cavity gas in LIB reactors. Recall that the high instantaneous heat flux is due to the unusually high transparency temperature of the noble gases. (3) The large temperature difference lasts for only a very short time and is also confined to a thin layer near the surface of the wall. This might be an advantage because only a small fraction of the wall experiences the thermal stress with the majority of the load carrying structure being unaffected. However, this localized stressing could also lead to cracking, etc. At this time there can be no clear-cut conclusion regarding the implications of this high instantaneous heat loading.

(*) Note that the power at 10 Hz is 10 x the power at 1 Hz.

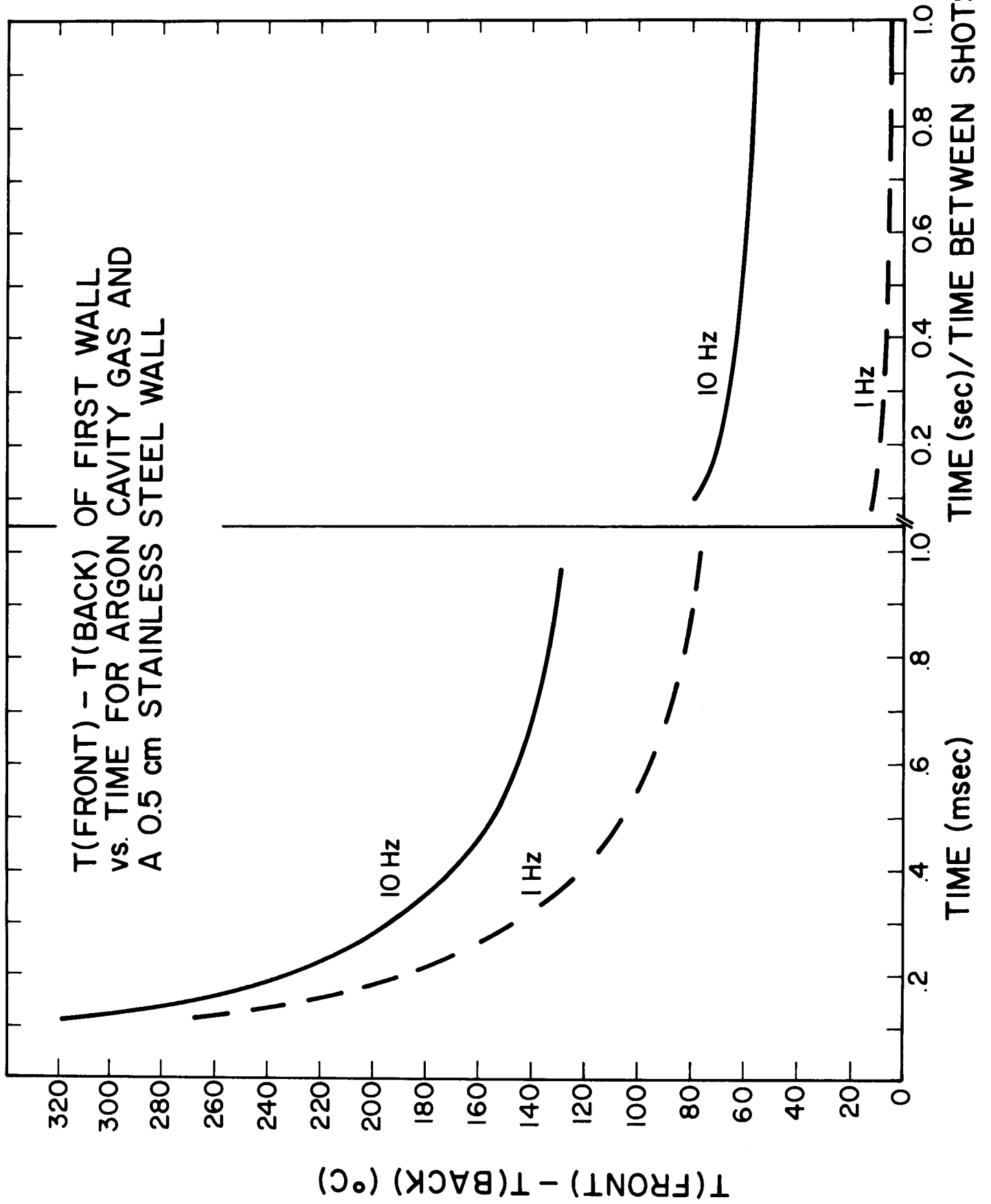
T(FRONT) – T(BACK) OF FIRST WALL
vs. TIME FOR ARGON CAVITY GAS AND
A 0.5 cm STAINLESS STEEL WALL
10 Hz
1 Hz
T(FRONT) – T(BACK) (°C)
TIME (msec)
TIME (sec)/TIME BETWEEN SHOTS

Fig. V-2

Recall that the heat flux behavior is entirely different for a non-noble gas. This was demonstrated with "diatomic argon" in Part III of this summary. Here the maximum heat flux and amount of energy radiated to the first wall is 10^2 times less than in the argon case. The thermal response of the wall for this case is shown in Fig. V-3. We can clearly see from these results that the wall thermal response is much more benign, 2.7°C maximum temperature rise as compared to 317°C for argon. This is now acceptable from a thermal stress point of view.

The results of these calculations are most important. They indicate that the thermal response of the wall is a limiting factor in the wall design. To allow the use of stainless steel as the structural material, a non-noble cavity gas is likely to be necessary.

References for Part V

1. S. I. Abdel-Khalik, "SOLASE - A Laser Fusion Reactor Study", UWFDM-220, Chapter X.

2. R. Richtmyer and K. Morton, Difference Methods for Initial Value Problems, Wiley, Chapter 8.

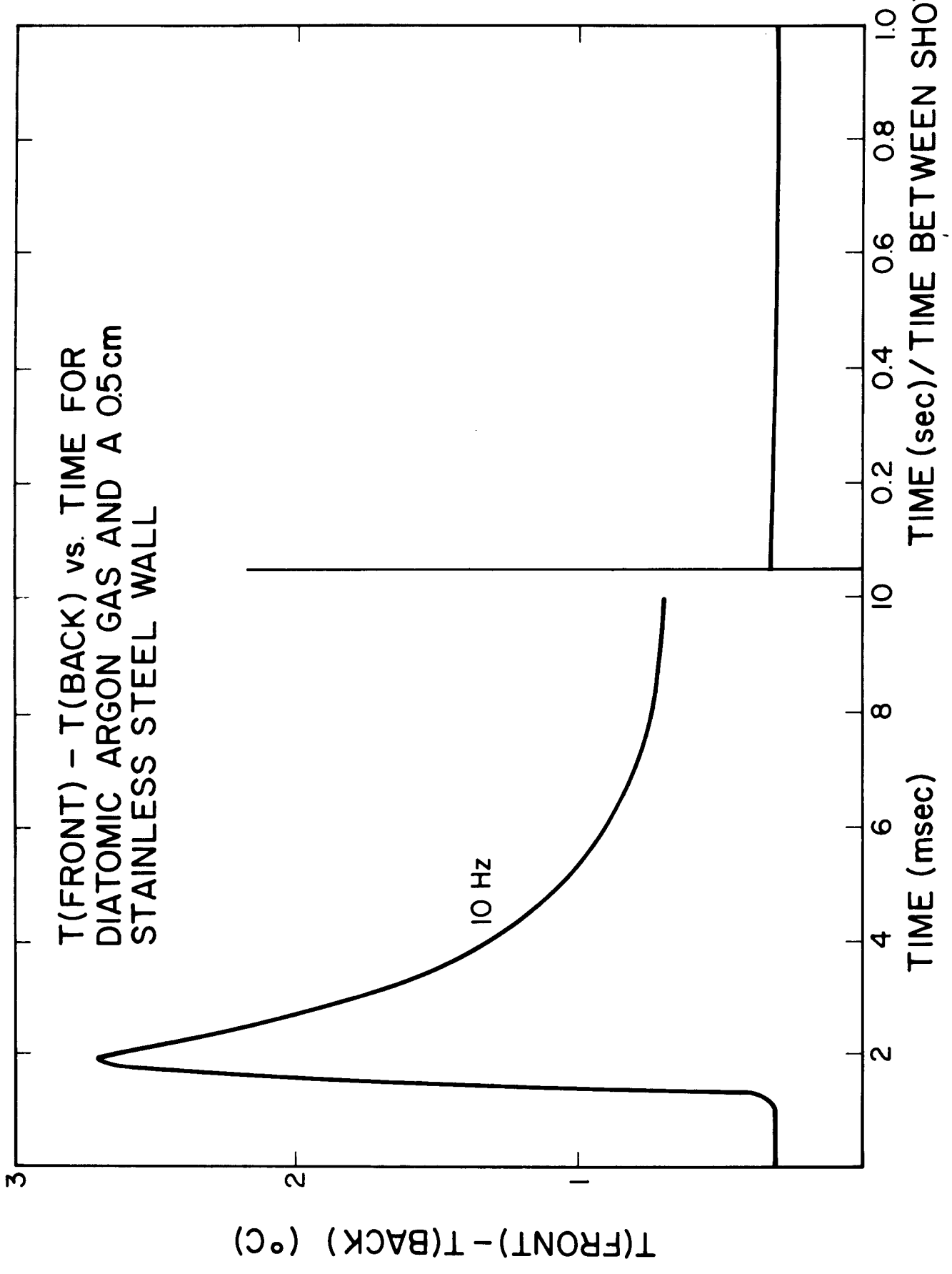
T(FRONT) – T(BACK) vs. TIME FOR
DIATOMIC ARGON GAS AND A 0.5cm
STAINLESS STEEL WALL
10 Hz
T(FRONT) – T(BACK) (°C)
TIME (msec)
TIME (sec) / TIME BETWEEN SHOTS
1
2
3
2
4
6
8
10
0.2
0.4
0.6
0.8
1.0

Fig. V-3

VI. Cavity Gas Recirculation System

In a LIB reactor, 20-30% of the target yield energy will be deposited in the cavity gas. Depending on the type of gas, this energy will be either quickly or slowly reradiated to the first wall. If the gas is not recirculated through a heat exchanger it will reach an equilibrium temperature in the cavity, where on each shot the same amount of energy radiates to the first wall as is deposited in the gas. This is demonstrated in Fig. IV-1 for argon gas. This figure shows the amount of energy radiated to the first wall for fireball calculations that start with different initial gas temperatures. In each case, 30 MJ of energy is added to the gas. It is seen that the equilibrium point is reached at a gas temperature of about 8500°K. For initial gas temperatures below this value there is less than 30 MJ radiated to the wall between shots. Hence, for the cavity gas to be in a cyclic steady-state at a temperature less than 8500°K, it must be recirculated so that heat can be removed by an external heat exchanger. The mass flow rates required to accomplish this are given in Table VI-1.

The simplest heat transfer system for this cavity gas is shown schematically in Fig. VI-2. There are a number of considerations that do not allow such a simple system to be practical. (1) The temperature of the exiting cavity gas is too high. Most gas-water heat exchangers work with gas temperatures of less than 1000°K.[1,2] For the gas temperature to be maintained at this low value the mass flow rate will be excessively high. (2) The pressure of the hot gas is too low for efficient pumping. To

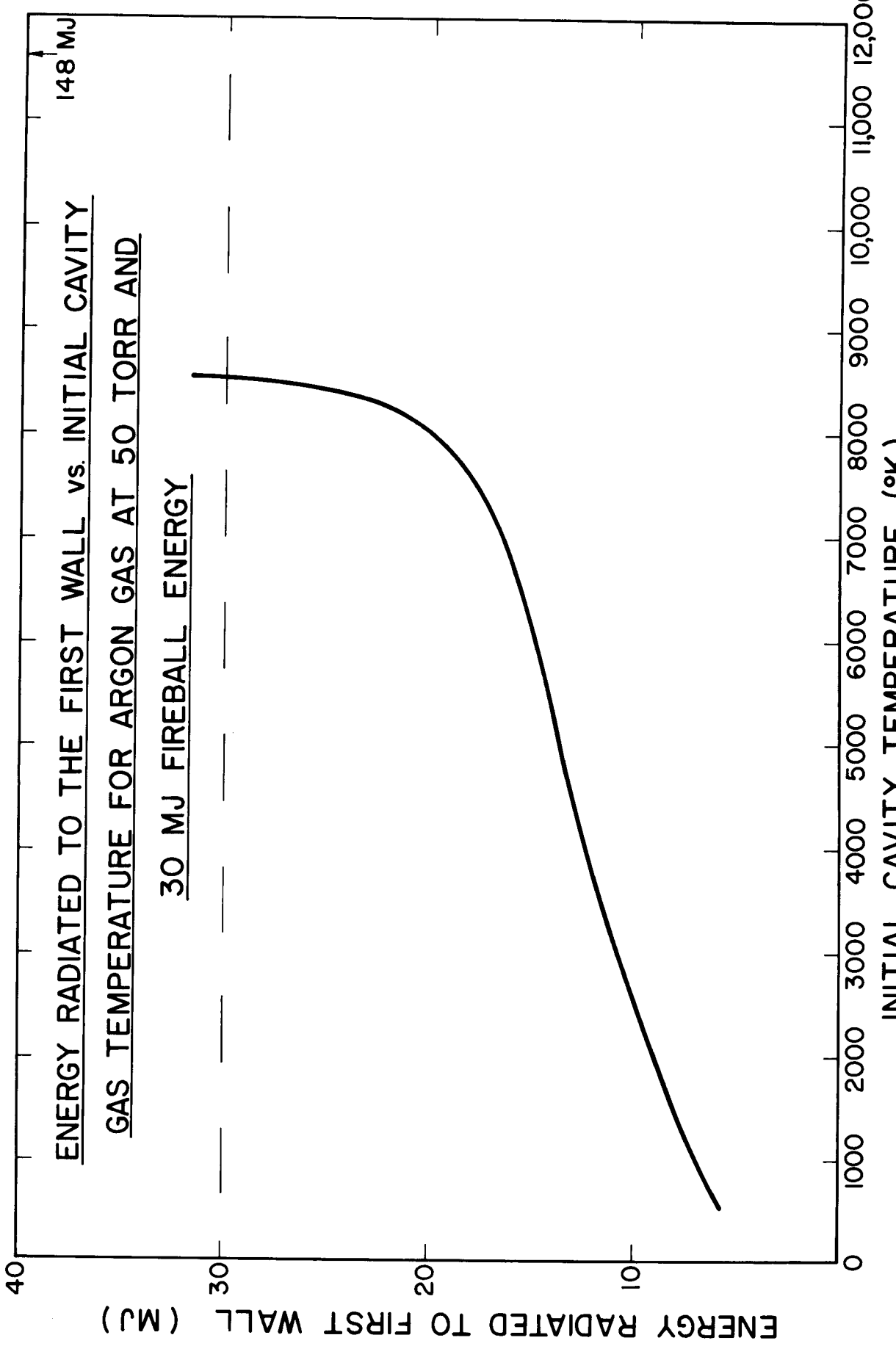
ENERGY RADIATED TO THE FIRST WALL vs. INITIAL CAVITY
GAS TEMPERATURE FOR ARGON GAS AT 50 TORR AND
30 MJ FIREBALL ENERGY
148 MJ
ENERGY RADIATED TO FIRST WALL (MJ)
INITIAL CAVITY TEMPERATURE (°K)
0
1000
2000
3000
4000
5000
6000
7000
8000
9000
10,000
11,000
12,000
10
20
30
40

Fig. VI-1

Table VI-1

Mass Flow Rates Required to Maintain Cavity Gas Temperature at Less Than 8200°K

Cavity Gas Temp. (°K)	$\dot{Q}_{IN}$ (MW)	$\dot{Q}_{WALL}$ (MW)	$\dot{Q}_{GAS}$ (MW)	C_P $(\frac{MJ}{g \cdot keV})$	$\dot{m}$ (g/sec)
580	30	6.6	23.4	6.4	2.7×10^6
1160	30	7.5	22.5	6.4	3.3×10^4
5802	30	14.6	15.2	6.4	2.5×10^3
8123	30	20.3	9.7	15.8	4.5×10^2

Argon gas at 50 torr (@0°C).

Assumes a repetition rate of 1 Hz and 30 MJ/shot deposited into the gas.

For 10 Hz all mass flow rates are x 10.

SIMPLE CAVITY GAS RECIRCU-LATION SYSTEM

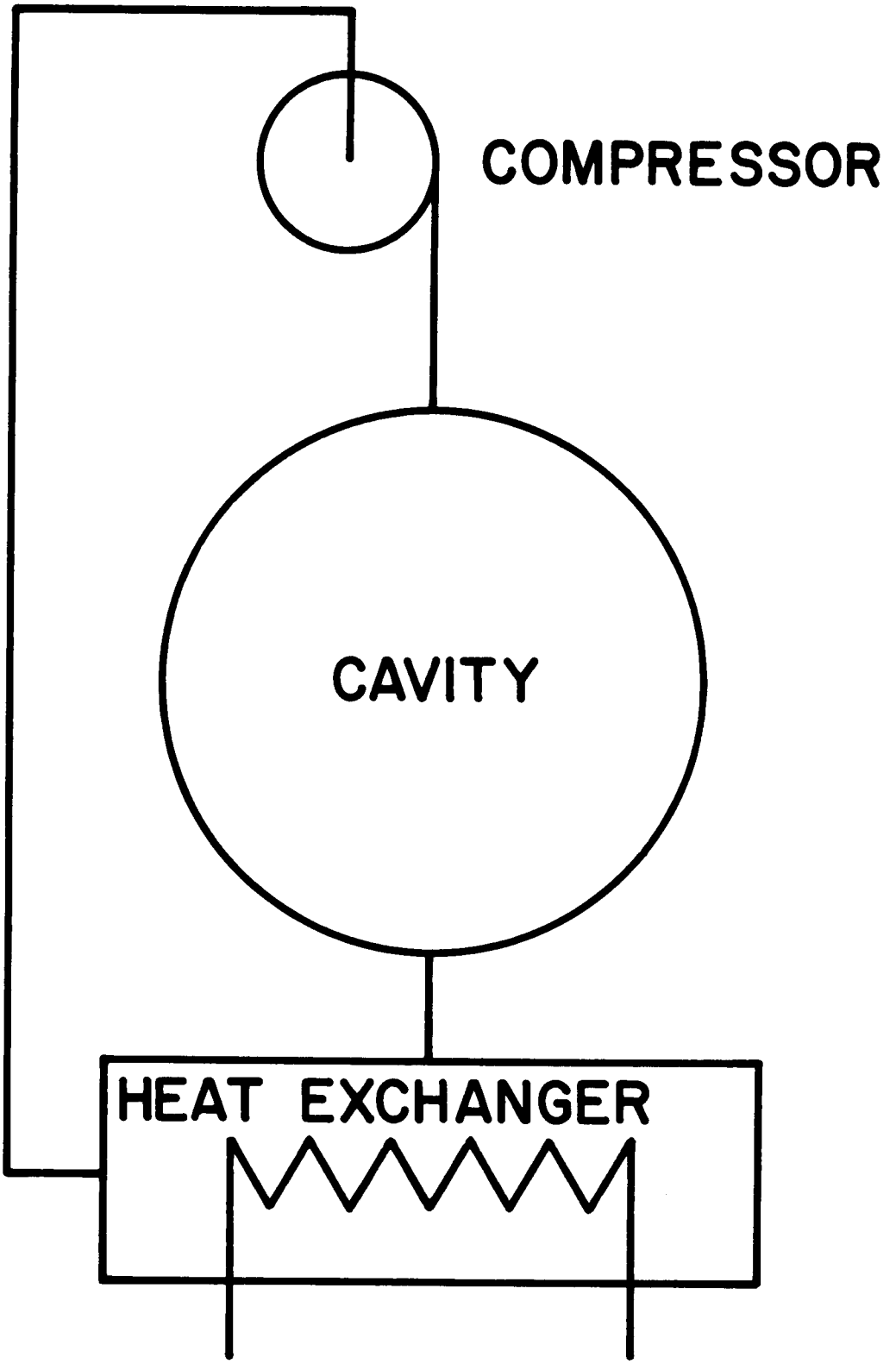

Fig. VI-2

pump gases at this low pressure and the required mass flow rates necessitates large pumping powers. (3) The pressure of the hot gas is too low for effective heat transfer. The gas pressure in an HTGR is 150 - 300 psi (~10-20 atmospheres) whereas it is only about 0.4 - 1.0 atmosphere in the LIB reactor. Hence the surface area needed to transfer heat at this pressure is very large, implying a very large heat exchanger. All of these problems lead to the conclusion that the simplest possible gas recirculation system will not be acceptable.

An alternative design that has the potential to solve many of these problems is shown schematically in Fig. VI-3. The main loops of the cycle are operated at high pressure just as an HTGR. A small fraction of the mass flow is passed through an expansion valve into the reactor cavity. This gas is heated to a high temperature in the cavity and is recombined with high pressure coolant flow after leaving the cavity. The cavity is pumped by a jet pump that also serves the remixing function. The mixed gas, now at an acceptable temperature, flows to a cross-flow heat exchanger. In this design the pressure and temperature of the gas are compatible with the main compressor and heat exchanger, making the cycle look very nearly like an HTGR cycle. The problems of handling low pressure, hot gas have not been eliminated but they have been isolated to a small part of the recirculation cycle. Special piping design will be necessary as well as special piping materials. Also, the jet pump must be designed. These are not the only problems encountered in the gas recirculation system. The suppression chamber at the inlet to the reactor is designed to suppress the shock that will propagate back up the gas duct when the target explodes.

CAVITY GAS RECIRCULATION SYSTEM

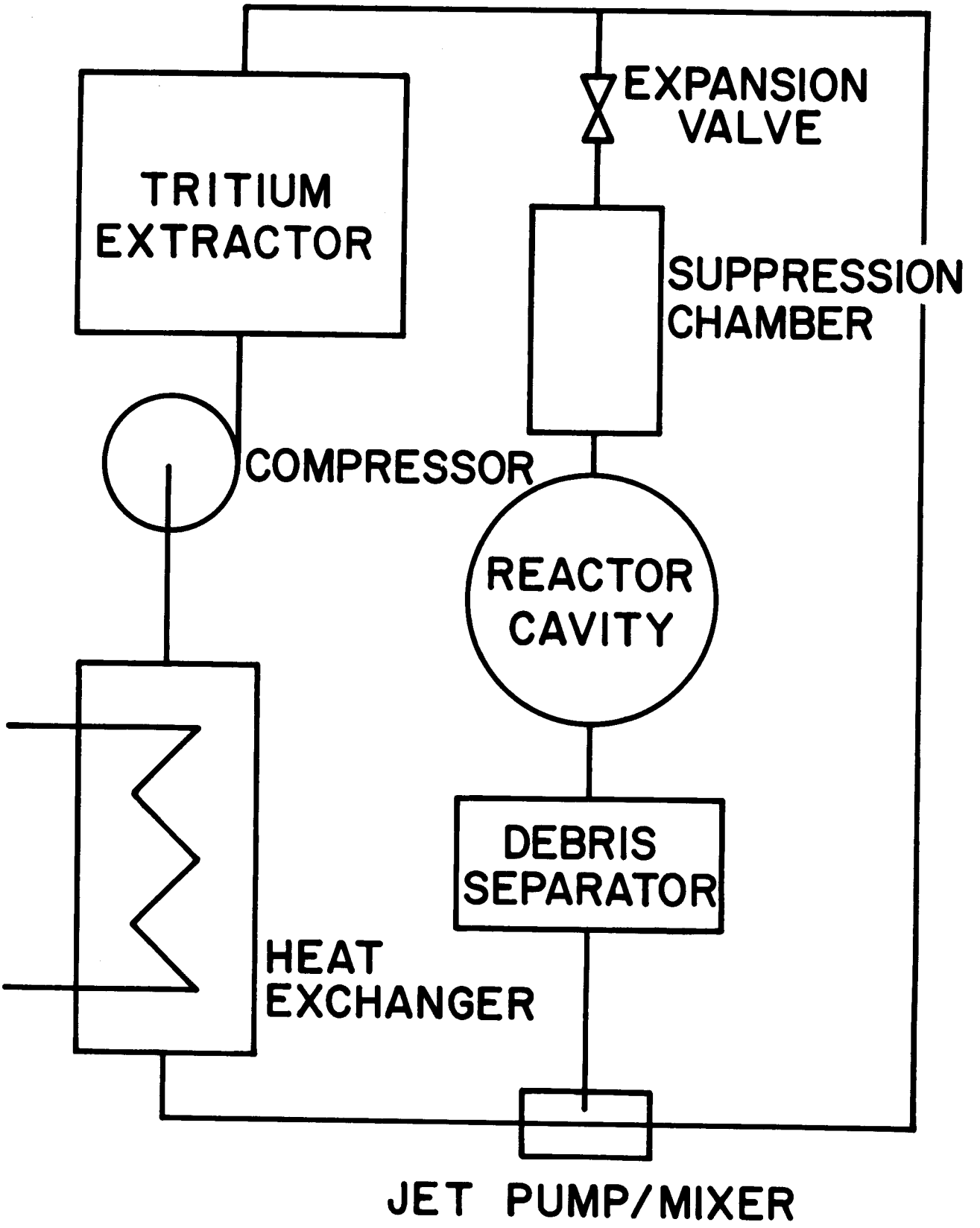

Fig. VI-3

The tritium separation equipment is of course needed to remove the unburnt tritium from the gas stream. The debris separator removes high temperature condensibles from the cavity gas before introduction into the main circulation loop. These components have not been designed in detail in this study. However investigation has been done to identify the problem areas discussed earlier.

References for Part VI

1. M. M. El-Wakil, private communication.

2. J. J. Duderstadt, Nuclear Reactor Analysis, Wiley (New York, 1976) Appendix H.

VII. Neutronics and Radiation Damage

A very important aspect of any DT fusion reactor design is the calculation of the transport of the 14.1 MeV fusion neutrons. These neutrons carry 70-80% of the reaction energy, hence the deposition of this energy in the blanket is important to the design of the heat transfer system. They are also used to breed tritium from Li in the blanket via the $^{6}Li(n,\alpha)^{3}T$ or $^{7}Li(n,\alpha n')^{3}T$ reactions. Furthermore, collisions between these high energy neutrons and the nuclei of the structural materials in the blanket result in displacement of these atoms from their lattice sites in the crystalline structure of the material. This displacement damage working in concert with the production of He and H gases in the structural material via (n,α) and (n,p) reactions results in so-called radiation damage effects. These can include loss of ductility and swelling of the structural material and they limit the useful lifetime of the material in the reactor.

In this study, neutronics calculations are done using both a time integrated and time dependent model of transport. Account is taken for neutron interaction in the pellet material surrounding the burning DT fuel along with interactions in the first wall and blanket. These calculations are described in detail in UWFDM-295.

The model pellet used for these calculations is shown in Fig. VII-1, with specific parameters given in Table VII-1. The model first wall and blanket are shown in Fig. VII-2. This study did not involve a detailed blanket design. However, the total neutron flux at the first wall is strongly determined by the blanket that is behind it. Therefore a "standard" blanket design is used for these calculations to give typical values for

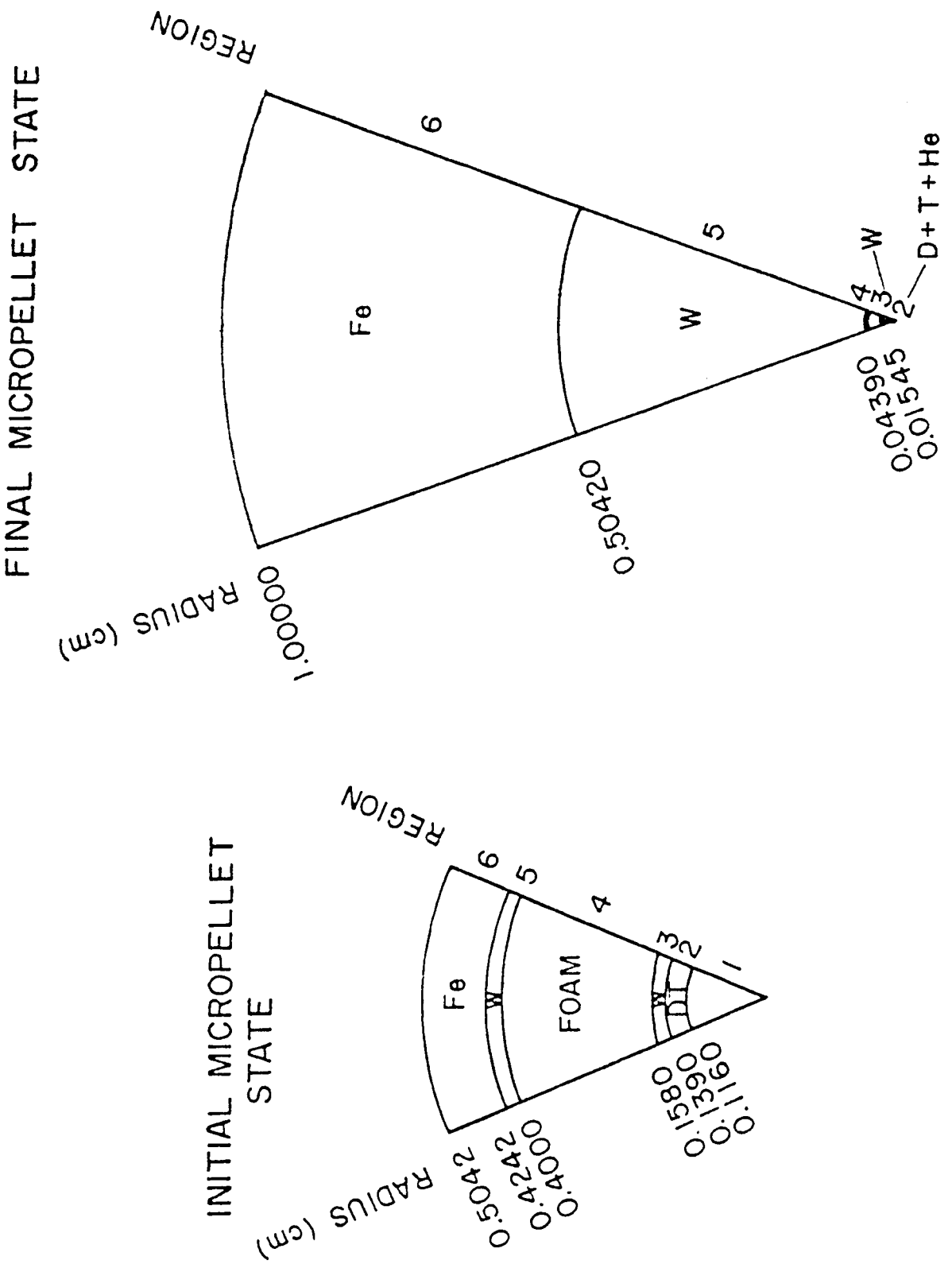
FINAL MICROPELLET STATE
REGION
RADIUS (cm)
Fe
W
D+T+He
6
5
4
3
2
1.00000
0.50420
0.04390
0.01545
INITIAL MICROPELLET STATE
REGION
RADIUS (cm)
Fe
W
FOAM
W
DT
6
5
4
3
2
1
0.5042
0.4242
0.4000
0.1580
0.1390
0.1160

Fig. VII-1

Table VII-1 Pellet Data for the Initial and Final States

Region	Composition	Volume(cm^3)	Initial Density (g/cm^3)	ρr (g/cm^2)	Material Weight(g)	Atomic Densities Atoms/(b·cm)
Initial State						
1	Void	6.54×10^{-3}	-	-	-	-
2	Frozen DT (50-50 atomic mixture	4.71×10^{-3}	0.213	4.90×10^{-3}	1.00×10^{-3}	$N_D = N_T = 2.55 \times 10^{-2}$
3	W Tamper	5.27×10^{-3}	19.300	3.67×10^{-1}	1.02×10^{-1}	$N_W = 6.32 \times 10^{-2}$
4	Foam Cushion	2.52×10^{-1}	-	-	-	-
5	W Pusher	5.17×10^{-2}	19.300	4.67×10^{-1}	9.98×10^{-1}	$N_W = 6.32 \times 10^{-2}$
6	Fe Ablator	2.17×10^{-1}	7.874	6.30×10^{-1}	1.71×10^{0}	$N_{Fe} = 8.49 \times 10^{-2}$
Sum		5.37×10^{-1}			2.81×10^{0}	
Imploded Final State						
Region	Composition	Volume(cm^3)	Final Density (g/cm^3)	ρr (g/cm^2)	Material Weight(g)	Atomic Densities Atoms/(b·cm)
2	D + T + ^4He	1.54×10^{-5}	6.10×10^{1}	9.42×10^{-1}	2.80×10^{-4} 4.20×10^{-4} 2.40×10^{-4}	5.44×10^{0} 5.45×10^{0} 2.35×10^{0}
3	W	3.39×10^{-4}	3.01×10^{2}	8.56×10^{0}	1.02×10^{-1}	9.86×10^{-1}
5	W	5.37×10^{-1}	1.86×10^{0}	8.56×10^{-1}	9.98×10^{-1}	6.09×10^{-3}
6	Fe	3.65×10^{0}	4.68×10^{-1}	2.32×10^{-1}	1.71×10^{0}	5.05×10^{-3}
Sum		4.19×10^{0}			2.81×10^{0}	

MATERIALS IDENTIFICATION

1 GRAPHITE
2 STAINLESS STEEL (100% d.f)
3 Li_2O (60%) + S.S. (2%)
4 B_4C (90%) + S.S. (10%)
1000 INNER VACUUM
0 OUTER VACUUM

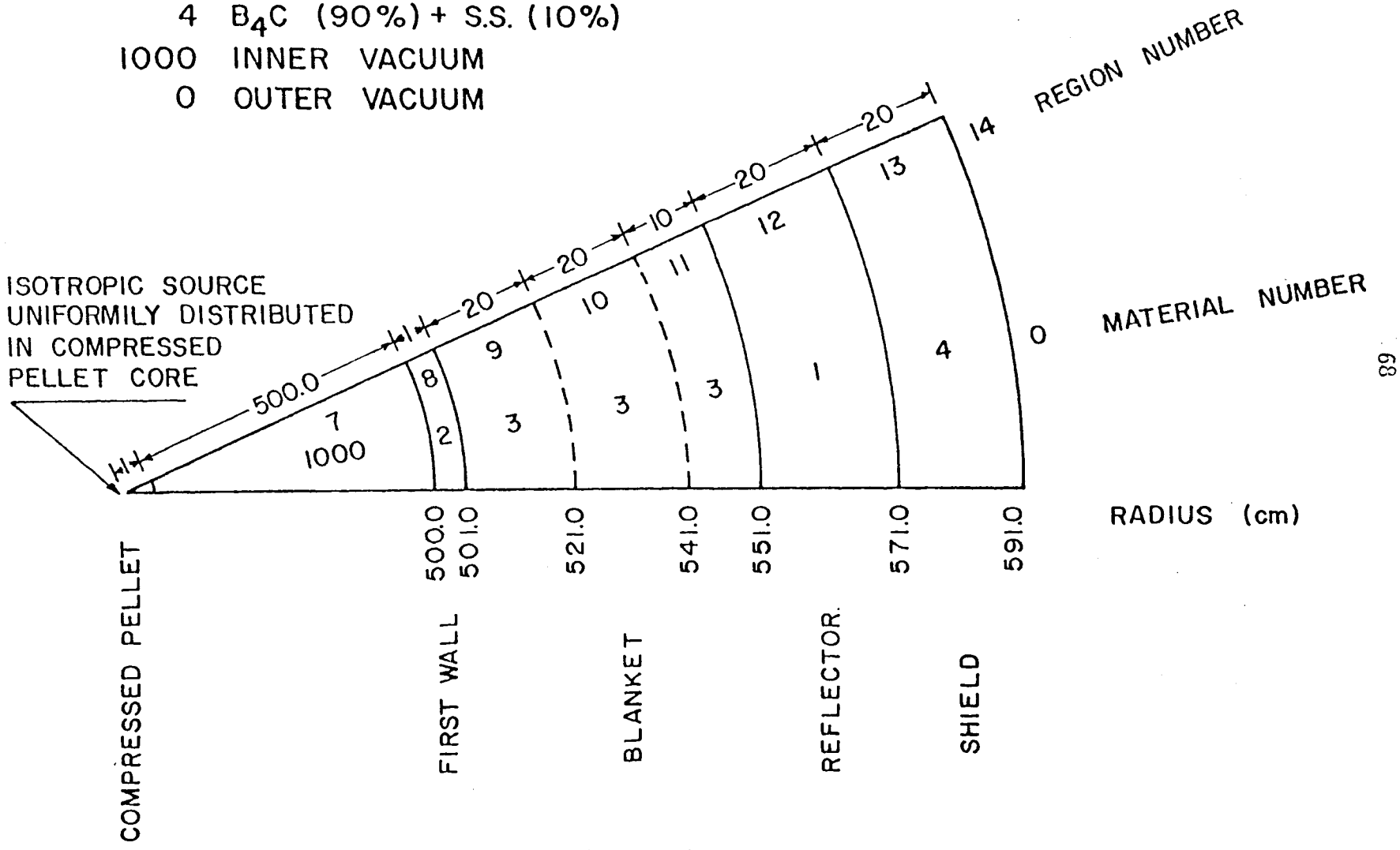

Fig. VII-2

the nuclear energy deposition, tritium production and radiation damage parameters for this reactor concept. These values are given in Tables VII-2 to VII-4 for different choices of the tamper material in the pellet. They are also compared to the case of no neutron interactions in the pellet, such as would be expected from a magnetically confined plasma. It can be seen that the tritium production and nuclear heating in the blanket are not affected very much by the presence of the pellet surrounding the DT fuel. The radiation damage parameters in the first wall are reduced by about 20%.

The parameters in Table VII-4 are useful in determining cumulative effects but they mask the true pulsed nature of the neutron damage. Of course the total damage per MW/m^2 is approximately the same when integrated over long times, but the pulsed damage has been shown by experiments[2-7] and theory[8-10] to significantly alter high temperature phenomena such as void swelling. In order to illustrate the transient nature of the damage, the neutron flux, dpa rate, and helium production rates have been plotted as a function of time for the first wall and graphite reflector regions. These quantities are given in Fig. VII-3 to VII-5 for the W pellet and time is measured from the time of birth of the first fusion neutron.

The dpa rate in Fig. VII-4 shows that the rate of damage in the first wall is above 1 dpa per second for 0.005 microseconds and the damage rate has fallen to less than 10^{-7} sec^{-1} after 10 microseconds. Data from Fig. VII-4 is replotted, on a finer timescale, in Fig. VII-6. Here we see the dpa rate for a monoenergetic 14.1 MeV neutron source, a pellet with a W tamper, and the W-pellet with 50 cm of Li between it and the stainless steel wall. The basic features of Fig. VII-6 are:

Table VII-4 Comparison of Radiation Damage Parameters for Different Pellet Compositions.

Region	W	Pb	Nat. U	Pure 14.1 MeV Source
	dpa/sec			
First Wall	5.13-08±8.65-10	5.00-08±4.51-09	5.22-08±1.41-09	5.40-08±2.35-09
Graphite Reflector	2.82-09±9.93-11	3.09-09±1.81-10	3.03-09±2.16-10	2.99-09±2.00-10
	Hydrogen Production			
First Wall	2.45-06±5.64-08	2.42-06±8.71-08	2.39-06±7.01-08	2.77-06±1.16-07
	Helium Production			
First Wall	8.67-07±2.17-08	8.60-07±3.48-08	8.40-07±2.58-08	1.01-06±4.54-08
Reflector	1.53-07±9.04-09	2.08-07±1.78-08	1.51-07±1.84-08	1.63-07±1.50-08

For a microexplosion yield of 100 MJ at a repetition rate of 1 Hz, the 14.1 MeV source strength is 3.55×10^{19} (neutrons/sec). First wall radius is 5 m.

Table VII-2 Comparison of Nuclear Energy Deposition for Different Pellet Compositions. (MeV/source neutron).

Region	W	Pb	Nat. U	Pure 14.1 MeV Source
	Neutron Heating			
First Wall	3.36-01±7.63-03	3.31-01±1.19-02	3.28-01±9.01-03	3.81-01±1.59-02
Blanket 1	6.91+00±3.94-02	6.90+00±9.30-02	7.20+00±1.10-01	7.11+00±6.95-02
2	3.08+00±2.85-02	3.15+00±8.55-02	3.28+00±5.75-02	3.10+00±7.14-02
3	9.13-01±1.64-02	9.45-01±3.42-02	1.00+00±3.74-02	9.05-01±3.33-02
Reflector	2.78-01±1.08-02	3.33-01±2.25-02	2.92-01±2.78-02	3.00-01±1.63-02
Subtotal	1.15+01±5.30-02	1.17+01±1.33-01	1.21+01±1.33-01	1.18+01±1.07-01
	Gamma Heating			
First Wall	1.23+00±2.31-02	1.12+00±6.20-02	1.30+00±6.37-02	1.21+00±4.60-02
Blanket 1	1.50+00±1.60-02	1.45+00±4.73-02	1.55+00±5.38-02	1.50+00±3.86-02
2	8.21-01±1.27-02	7.62-01±2.36-02	8.17-01±3.11-02	7.63-01±1.97-02
3	2.39-01±5.95-03	2.10-01±1.16-02	2.20-01±1.20-02	2.20-01±1.11-02
Reflector	4.35-01±1.12-02	4.24-01±2.65-02	4.53-01±2.31-02	4.04-01±2.02-02
Subtotal	4.23+00±3.33-02	3.97+00±8.65-02	4.34+00±9.27-02	4.10+00±5.73-02
	Total Heating			
First Wall	1.57+00±2.43-02	1.45+00±6.31-02	1.63+00±6.43-02	1.59+00±4.87-02
Blanket 1	8.41+00±4.26-02	8.35+00±1.04-01	8.75+00±1.22-01	8.61+00±8.00-02
2	3.90+00±3.12-02	3.91+00±8.87-02	4.10+00±6.54-02	3.86+00±7.41-02
3	1.15+00±1.74-02	1.16+00±3.61-02	1.22+00±3.93-02	1.13+00±3.51-02
Reflector	7.13-01±1.56-02	7.57-01±3.48-02	7.45-01±3.61-02	7.04-01±2.60-02
TOTAL	1.57+01±6.26-02	1.57+01±1.59-01	1.64+01±1.62-01	1.59+01±1.26-01

Table VII-3 Comparison of Tritium Production Per Source Neutron for Different Pellet Compositions in Blanket Region (tritons/source particle).

Zone	W Pusher-Tamper	Pb Pusher-Tamper	Nat. U Pusher-Tamper	Pure 14.1 MeV Source
	^{7}Li Contribution			
1	2.79-01±2.88-03	2.57-01±5.07-03	2.78-01±6.88-03	3.11-01±4.93-03
2	1.05-01±1.90-03	9.88-02±4.91-03	1.04-01±5.42-03	1.11-01±4.36-03
3	2.06-02±7.28-04	1.79-02±1.54-03	2.01-02±1.56-03	2.14-02±1.17-03
Subtotal	4.05-01±3.53-03	3.74-01±7.22-03	4.02-01±8.90-03	4.43-01±6.68-03
	^{6}Li Contribution			
1	4.16-01±3.89-03	3.88-01±7.83-03	4.64-01±8.32-03	3.71-01±5.58-03
2	2.59-01±2.57-03	2.51-01±4.66-03	2.91-01±4.92-03	2.43-01±4.80-03
3	1.13-01±1.67-03	1.18-01±3.79-03	1.28-01±3.65-03	1.09-01±3.42-03
Subtotal	7.88-01±4.95-03	7.57-01±9.91-03	8.73-01±1.03-02	7.23-01±8.12-03
Total	1.19+00±6.08-03	1.13+00±1.23-02	1.28+00±1.36-02	1.17+00±1.05-02

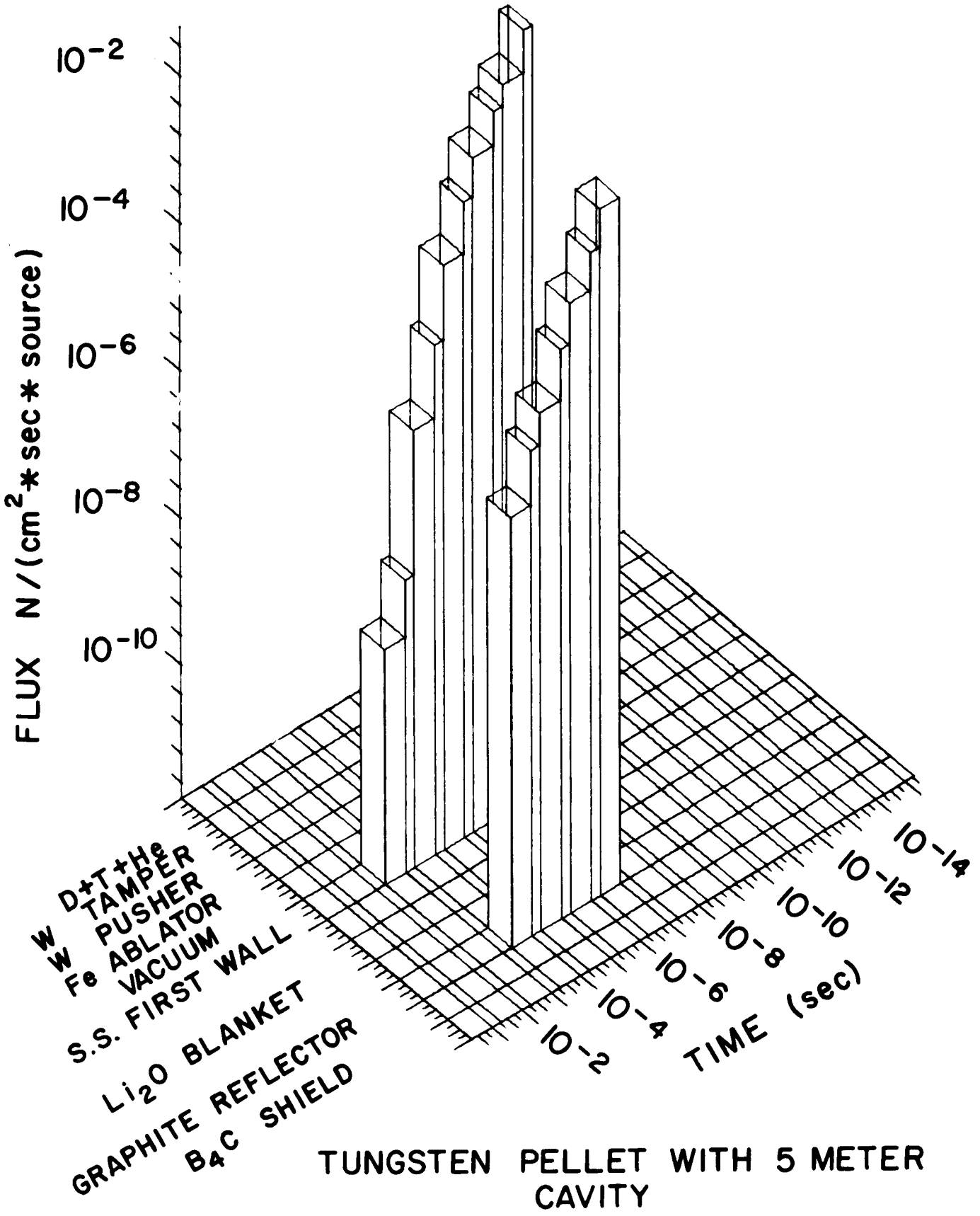

TUNGSTEN PELLET WITH 5 METER CAVITY

Fig. VII-3

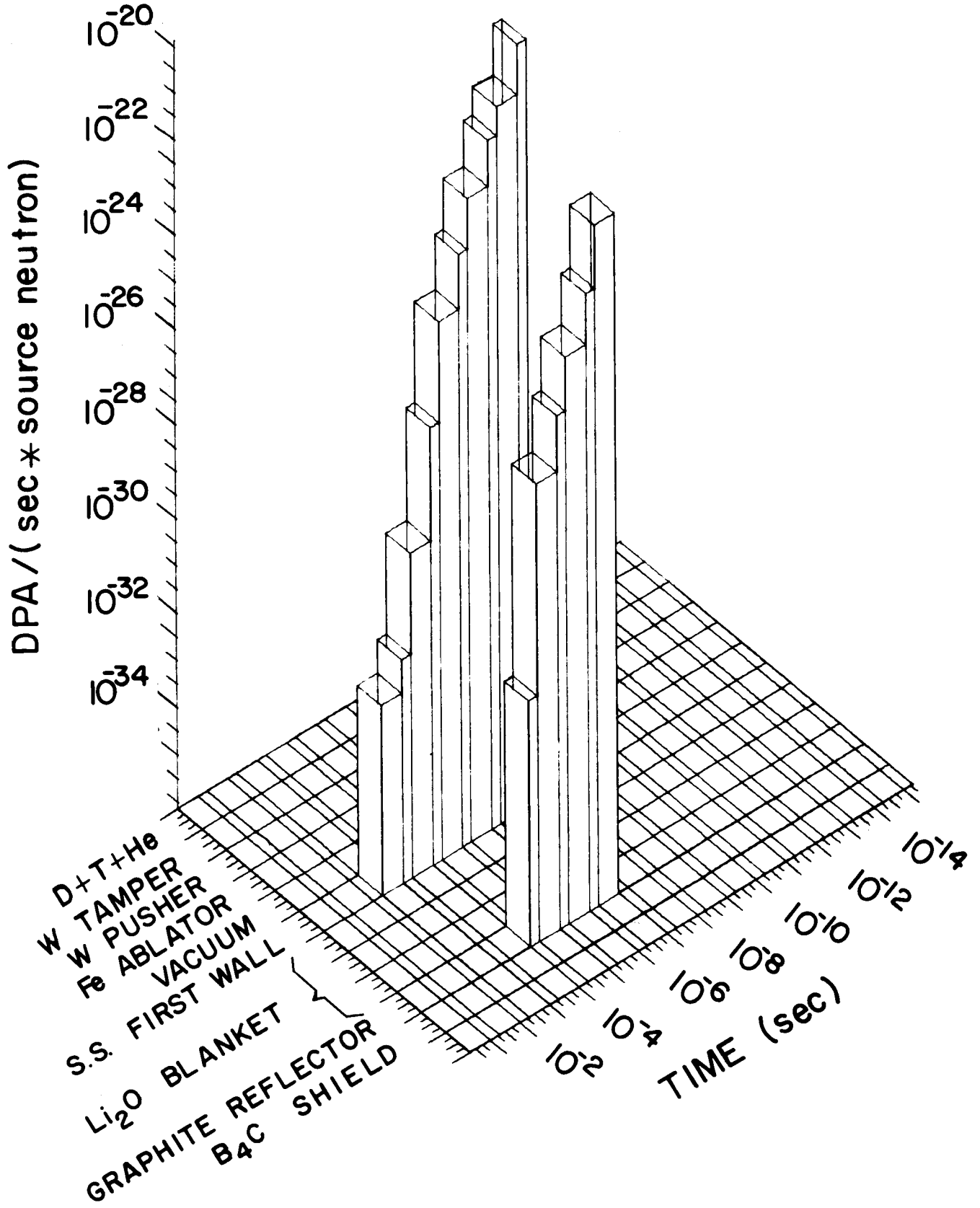

TUNGSTEN PELLET WITH 5 METER CAVITY

Fig. VII-4

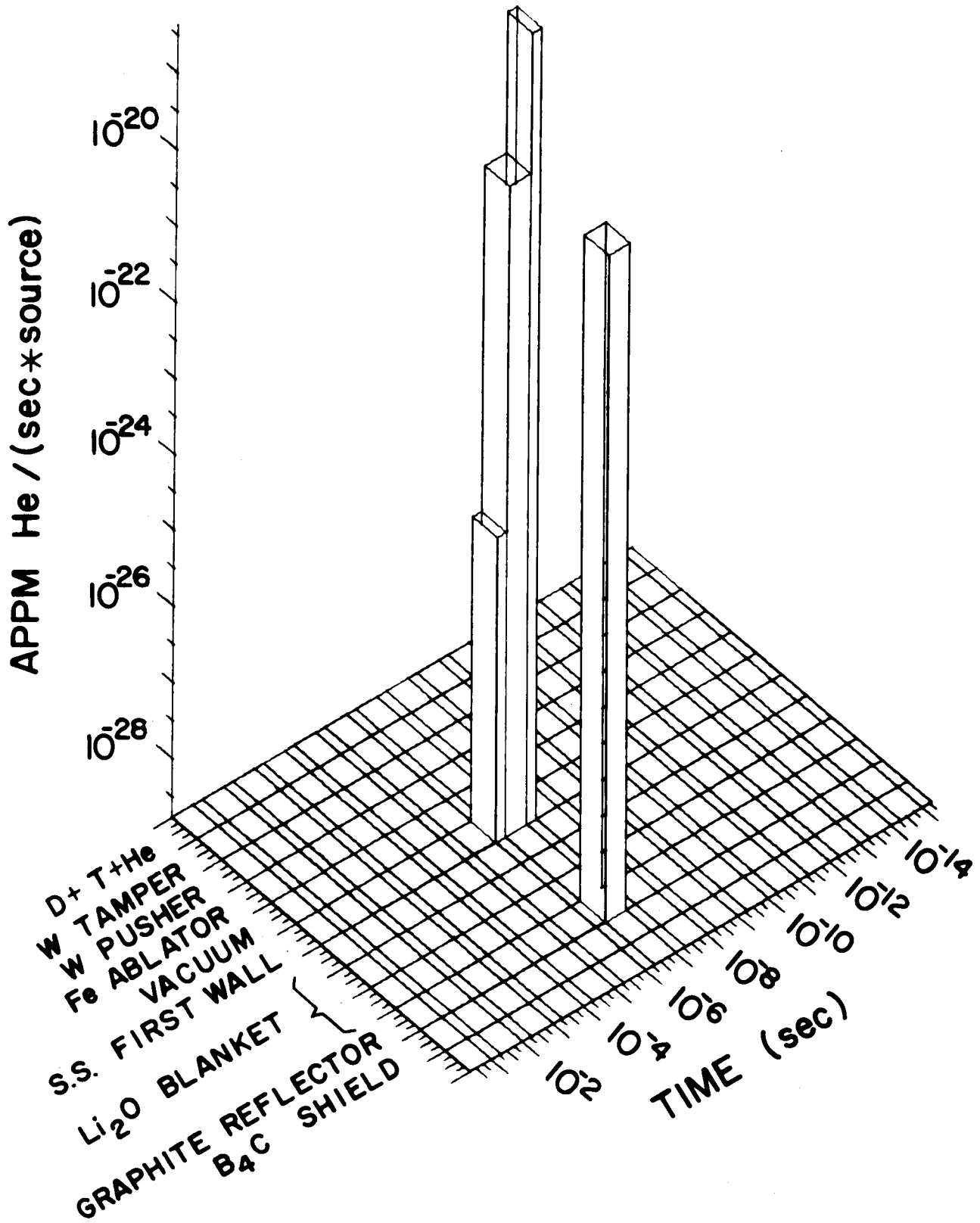

TUNGSTEN PELLET WITH 5 METER CAVITY

Fig. VII-5

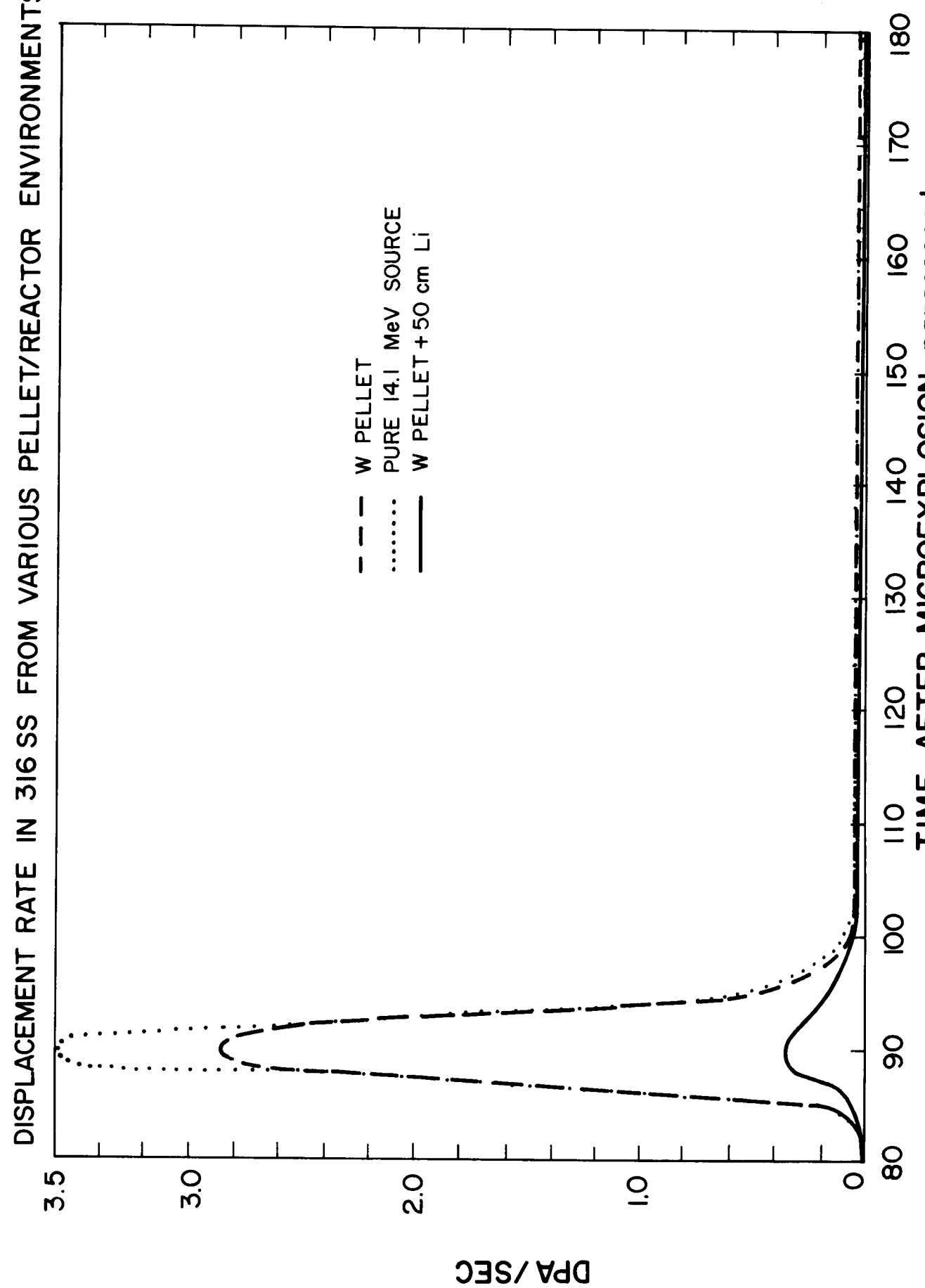
DISPLACEMENT RATE IN 316 SS FROM VARIOUS PELLET/REACTOR ENVIRONMENTS
W PELLET
PURE 14.1 MeV SOURCE
W PELLET + 50 cm Li
DPA/SEC
3.5
3.0
2.0
1.0
0
80
90
100
110
120
130
140
150
160
170
180
TIME AFTER MICROEXPLOSION, nanoseconds

Fig. VII-6

1. Most of the damage is done in a 316 SS wall within 15 ns after the most energetic neutrons strike the first wall.

2. The inclusion of the W in the pellet tends to reduce the peak damage rate by ~20% because of downscattering and time of flight spreading of the neutrons.

3. The damage rate behind a 50 cm thick Li zone is reduced a factor of ten from the first wall.

The significance of the third point is that one must be concerned about high dpa rates even well away from the first wall and any process that is sensitive to the dpa rate (e.g., creep or void swelling) will be affected well into the reactor blanket.

Another way to look at the data in Fig. VII-4 and VII-6 is to plot the fraction of displacement damage done above a given dpa rate. This is shown in Fig. VII-7 and it reveals that there is only a small difference between "bare" pellets and highly tamped ones. For example, while the maximum damage rate is 3 to 3.5 dpa/sec, only 1/4 of the total displacement damage is done at displacement rates of 1 dpa per second or more. It is also found that 50% of the damage is done above 0.1 dpa sec^{-1} and 90% of the damage is done above 0.01 dpa sec^{-1}. Examination of the damage behind a 50 cm Li zone reveals that there is still 50% of the total damage accumulated at the rate of 0.04 dpa sec^{-1} or higher. As a point of reference,[1] the typical displacement damage rates in magnetic fusion reactor first walls are a few times 10^{-7} dpa sec^{-1}.

The significance of higher damage rates is easily illustrated by two examples. The first is shown in Fig. VII-8 where the peak of void swelling in nickel is replotted as a function of damage rate. An increase in the <u>steady-state</u> damage rate of 10^5 (from 10^{-7} sec^{-1} to 10^{-2} sec^{-1}) causes the

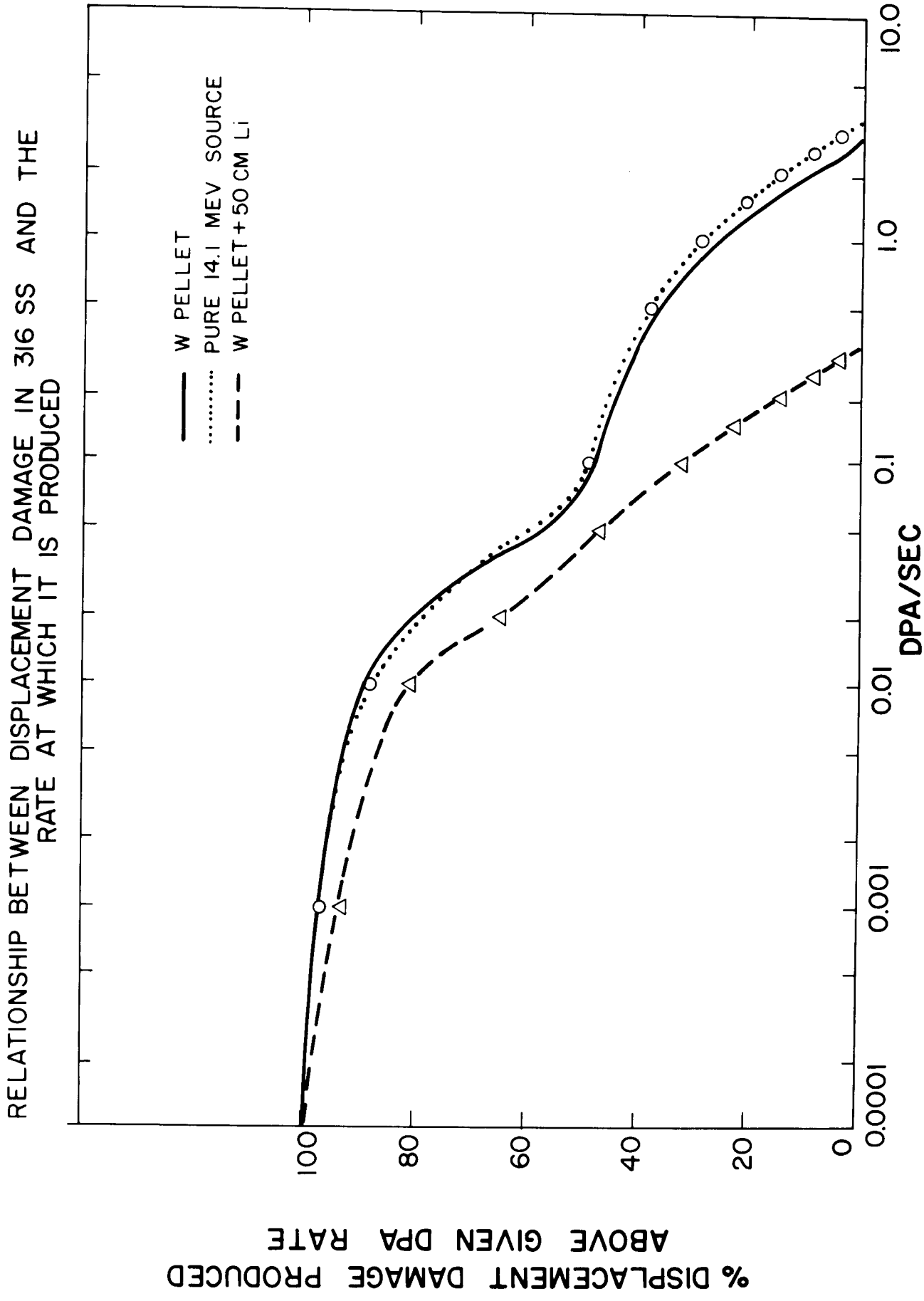
RELATIONSHIP BETWEEN DISPLACEMENT DAMAGE IN 316 SS AND THE RATE AT WHICH IT IS PRODUCED
W PELLET
PURE 14.1 MEV SOURCE
W PELLET + 50 CM Li
% DISPLACEMENT DAMAGE PRODUCED ABOVE GIVEN DPA RATE
100
80
60
40
20
0
0.0001
0.001
0.01
0.1
1.0
10.0
DPA/SEC

Fig. VII-7

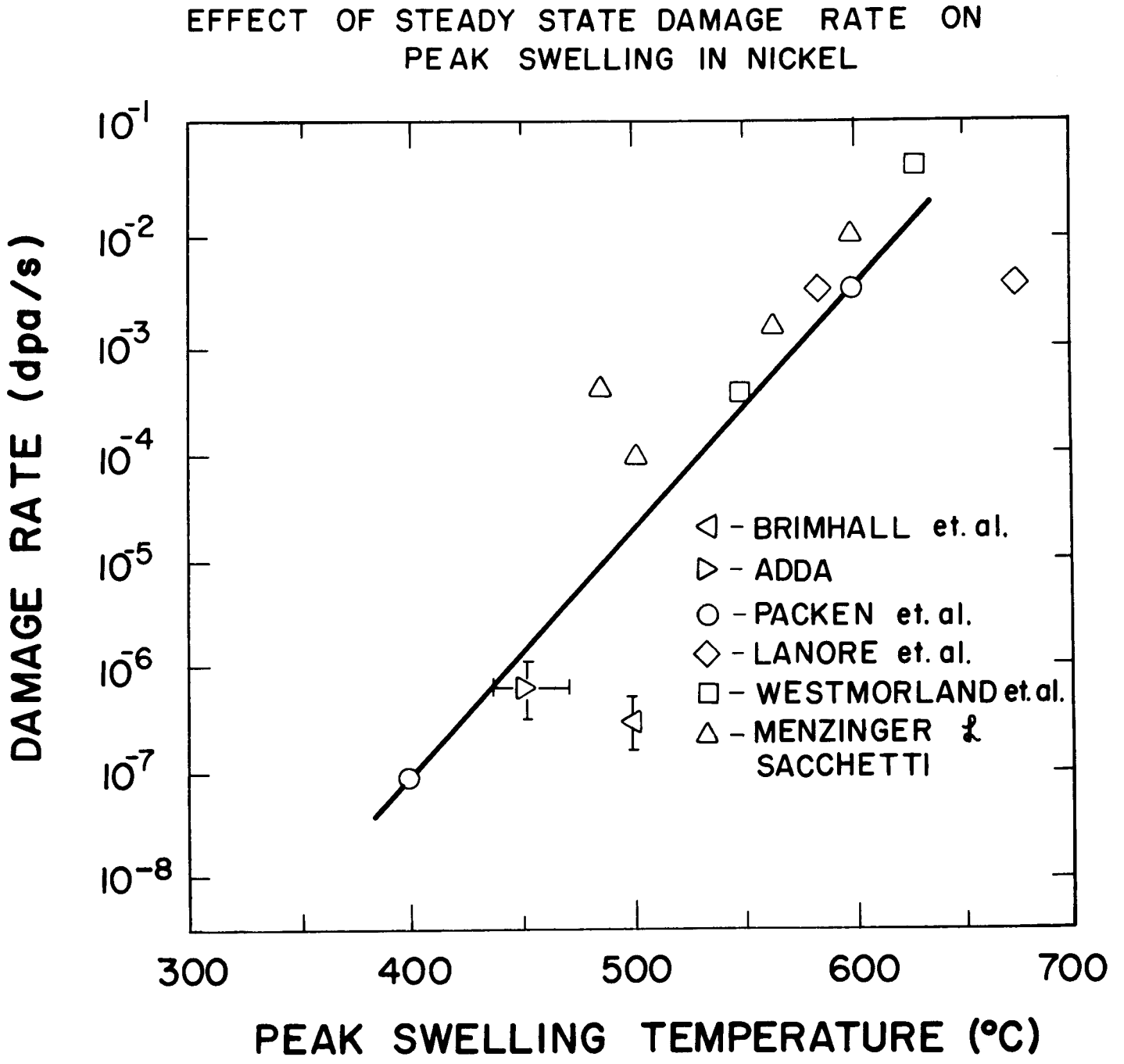

Fig. VII-8

Effect of damage rate on the peak swelling temperature of pure nickel. Note how the increase in dpa rate by a factor of 100,000 increases the peak swelling temperature by over 200°C.[13]

maximum swelling temperature to be increased by 200°C.[12] This same effect is shown in Fig. VII-9[13] where the swelling in 304 SS at 450°C is >10% for a steady-state dpa rate of 10^{-6} sec^{-1}. However, if the steady-state dpa rate is increased to 10^{-2} sec^{-1}, then there is essentially no swelling at 450°C.

There are five other experiments which illustrate the effect of not only high dpa rates but also of pulsed irradiation typical of ICF reactor operations.[3-7] These experiments are reviewed elsewhere,[14] but they reveal that the microstructure can be drastically altered depending on the temperature between damage pulses, and the time between pulses. Theoretical analyses[8-10] also confirm this complex materials behavior.

Because these problems are unique to inertial confinement fusion, the substantial body of data and theoretical analysis in support of the magnetic fusion approach do not necessarily carry over. For this reason, estimation of the first wall lifetime cannot be made with the same degree of confidence until further analysis is done on the pulsed nature of radiation damage.

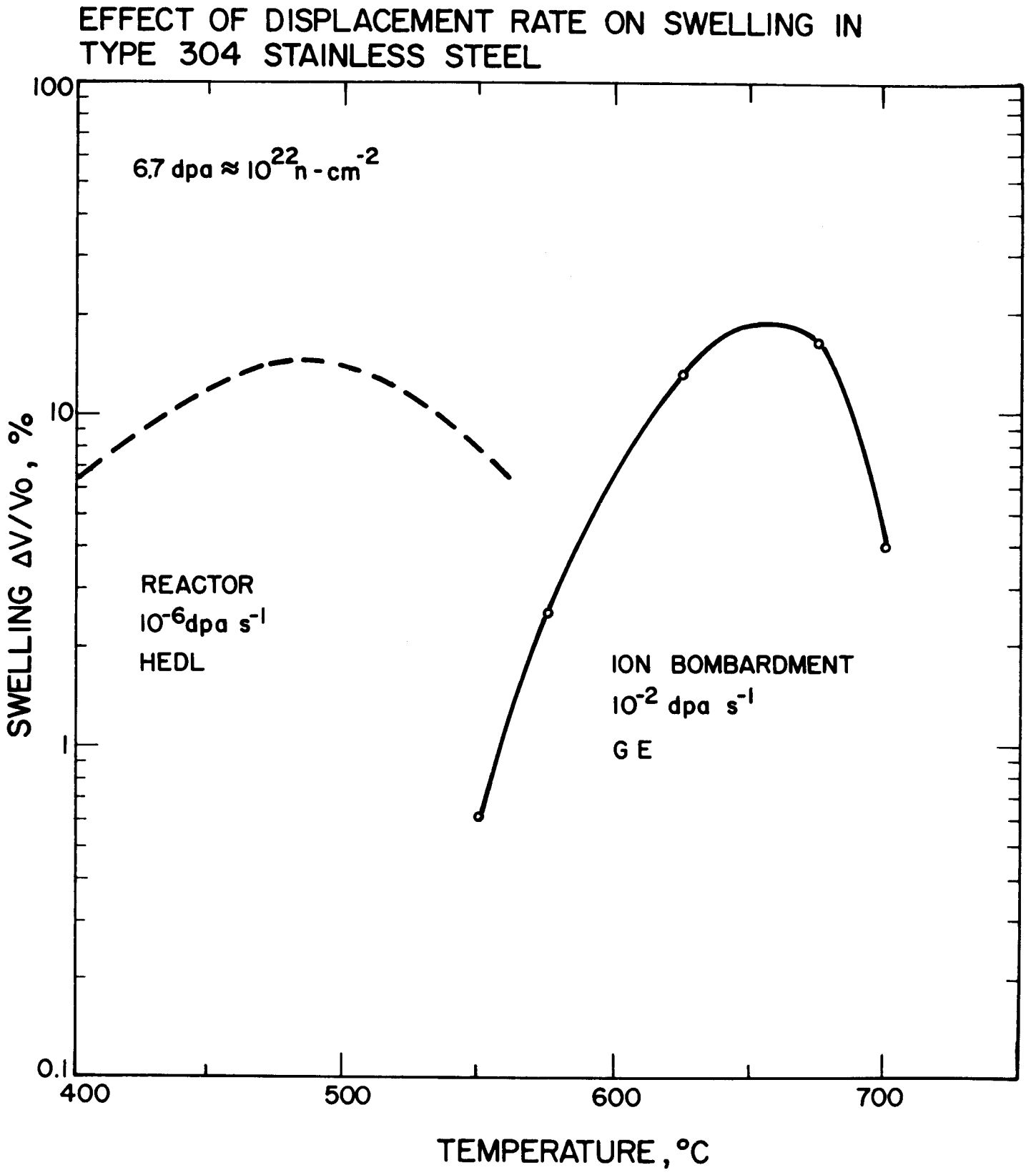

Fig. VII-9
Effect of displacement rate on swelling in 304 stainless steel. Note how a factor of 10,000 increase in dpa rate increases the threshold, maximum and upper limit.(14)

References for Part VII

1. G.L. Kulcinski, Proc. 3rd Topical Meeting on Tech. Contr. Nucl. Fusion, ed. J.R. Powell, CONF-780508, 598, 1979.

2. J.A. Sprague, and F.A. Smidt, Jr., NRL Memorandum Report 2629, 1973.

3. A. Taylor et al., Argonne National Laboratory Report, ANL/CTR/TM-39, 1975.

4. A. Taylor, D. I. Potter, and H. Wiedersich, Argonne National Laboratory Report, ANL/FPP-79-3, 1979.

5. T. Ryan, Ph.D. Thesis, Univ. of Michigan, 1974.

6. R.W. Powell and G.R. Odette, to be published, Proc. 1st Topical Meeting on Fusion Reactor Materials, Jan. 29-31, 1979.

7. D. Kaletta, ibid.

8. N.M. Ghoniem and G.L. Kulcinski, J. Nucl. Mat., 82, 392, 1979.

9. N.M. Ghoniem and G.L. Kulcinski, Nucl. Engr. Design, 52, 111, 1979.

10. N.M. Ghoniem and G.L. Kulcinski, J. Nucl. Mat., to be published.

11. M.M.H. Ragheb, G.A. Moses, and C.W. Maynard, University of Wisconsin Report UWFDM-295, July 1979.

12. N. Packen et al., J. Nucl Mat., 78, 143, 1978.

13. W.E. Johnston et al., Effects of Radiation on Substructure and Mechanical Properties of Metals and Alloys, ASTM-STP-529, Philadelphia, 213, 1973.

14. N.M. Ghoniem and G.L. Kulcinski, "A Critical Assessment of the Effects of Pulsed Irradiation on Materials," University of Wisconsin Report UWFDM-311, August 1979.

Acknowledgements

The authors wish to acknowledge the helpful discussions and support from the particle beam fusion division of Sandia Laboratories. In particular, we wish to thank Drs. Donald Cook and Mary Ann Sweeney who have directly participated in the definition of this work.

Funding for this work was provided by Sandia Laboratories, under contract to the US Department of Energy.